Applied Energy 391 (2025) 125876

Contents lists available at ScienceDirect

Applied Energy

journal homepage: www.elsevier.com/locate/apenergy

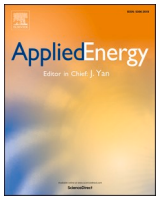

Investigating the partial load of reversible solid oxide cell systems: A focus on balance of plant and thermal integration

Marco Ficili, Paolo Colbertaldo *, Stefano Campanari, Giulio Guandalini

Group of Energy Conversion Systems (GECoS), Department of Energy, Politecnico di Milano - Via Lambruschini 4A, Milan 20156, Italy

HIGHLIGHTS

- Design of a rSOC system with balance of plant and molten salt thermal energy storage.
- Strategies to allow wide operating windows in both modalities are proposed.
- Comparison of different high-temperature heat provision configurations.
- Definition of system efficiency losses with respect to stack efficiency.
- Operating maps are obtained for fuel cell and electrolysis modalities.

ARTICLE INFO

Keywords:
Reversible solid oxide cells
Energy storage
Thermal storage
Molten salt
Partial load

ABSTRACT

Solid oxide cells are promising electrochemical devices capable of operating in both electrolysis and fuel cell modes with high electrical efficiency. This work investigates the design and partial-load operation of a reversible solid oxide cell (rSOC) system for steam electrolysis and hydrogen-based power generation, when adopting a unified balance of plant for both modes and molten salt thermal energy storage for thermal integration. Different configurations are compared with the aim of widening the part-load window, taking into account the electrochemical behavior as well as the changes in heat exchange properties. The definition of system efficiency losses with respect to the stack efficiency is proposed, helping in identifying the main causes of efficiency degradation throughout the part-load window. Results show that pre- or post-stack heaters are required when switching from exothermic to endothermic conditions. Moreover, they prove essential in keeping the rSOC in thermal balance also when the reaction is slightly exothermic. The use of electric heaters and hydrogen combustors is compared, and electric heaters appear to have the least impact on system efficiency at lower loads. For all configurations, the highest efficiency is obtained close to the thermoneutral point, which optimizes the trade-off between stack efficiency and system efficiency losses. Heat recovery in fuel cell mode is prominent at nominal load and could be beneficial in facilitating thermal integration between the two operational modes. However, the magnitude of its reduction at partial load is greater than the corresponding reduction in heat demand in electrolysis mode, leading to increased thermal imbalances between fuel cell and electrolysis modes.

1. Introduction

Solid oxide cell (SOC) systems are receiving increasing attention by the research and industrial communities due to their potential applications for energy storage and Power-to-X purposes [1]. With respect to the low-temperature counterparts, like polymer-electrolyte membrane and alkaline cells, they benefit from increased efficiency thanks to their high operating temperature (600–900 °C). Conventional materials adopted in solid oxide cells include mixtures of nickel and yttria-stabilized zirconia (YSZ) for the fuel electrode, lanthanum strontium cobaltite (LSC) for the oxygen electrode, and a solid electrolyte made of YSZ. The high operating temperature and the presence of nickel on the fuel side gives SOCs the interesting capability of processing carbon-containing species like natural gas or syngas with reduced risk of carbon deposition, in presence of sufficient amounts of water. Given the gaseous nature of the reactants and the materials adopted, SOCs can seamlessly operate as solid oxide fuel cell (SOFC) and solid oxide electrolysis (SOEC) mode within a single device. In this regard, they take the name of reversible solid oxide cells (rSOCs). They may represent a

* Corresponding author.
E-mail address: paolo.colbertaldo@polimi.it (P. Colbertaldo).

https://doi.org/10.1016/j.apenergy.2025.125876
Received 5 August 2024; Received in revised form 15 March 2025; Accepted 4 April 2025
Available online 18 April 2025

Nomenclature

AC	Alternating current
ASR	Area-specific resistance
BoP	Balance of plant
CHP	Combined heat and power
CSP	Concentrated solar power
DC	Direct current
EC	Electrolysis
EH	Electric heater
FC	Fuel cell
HC	Hydrogen combustor
HX	Heat exchanger
LSC	Lanthanum strontium cobaltite
OCV	Open-circuit voltage
PCM	Phase-change material
Post-EH	Electric post-heater
Post-HC	Post-combustor fed with hydrogen-rich fuel exhaust
Pre-EH	Electric pre-heater
Pre-HC	Pre-combustor fed with hydrogen-rich fuel exhaust
P2P	Power-to-Power
rSOC	Reversible solid oxide cell
SOC	Solid oxide cell
SOEC	Solid oxide electrolysis cell
SOFC	Solid oxide fuel cell
TES	Thermal energy storage
VFD	Variable-frequency drive
YSZ	Yttria-stabilized zirconia

fundamental component in large-scale storage systems, in competition with technologies based on lithium-ion batteries as they could prove cost-effective in the long run on large time shift applications, and with mechanical technologies like compressed air energy storage or pumped hydro storage due to lower geographical and site-specific constraints. On top of the storage application, rSOCs can also be coupled to industrial applications as the produced hydrogen or syngas can serve as valuable feedstock for downstream processes.

There is wide evidence of the performances of single cells or short stacks of solid oxide cells operated in a reversible way in a laboratory environment (furnace at controlled temperature). At lab scale, the reversible operation has proved beneficial in reducing or even eliminating major degradation mechanisms that occur within a continuous application in single mode [2–4]. On other hand, there are few instances of experimental studies on complete systems including the required balance of plant (BoP) that are self-sustaining in keeping a stable thermal balance among the system components, ensuring adequate operating temperatures [5–7]. Nonetheless, an increasing number of studies have begun investigating the design, required characteristics, and performances of rSOC systems with the aid of numerical models. One of the main challenges in the design of such systems resides in the thermal integration between the two modalities. When operated in EC mode, the water evaporation process requires a large amount of heat. Moreover, at particularly low current densities and low operating voltages, the electrolysis reaction becomes endothermic and requires external high-temperature heat provision. Both these needs can sensibly affect the system efficiency. On the contrary, during FC mode, the oxidation reaction is extremely exothermic and excess heat is available to be stored for later use. In the following section, a review of the available studies on rSOC systems is presented, with a focus on the strategies to manage the thermal integration issues.

1.1. Review on rSOC systems

Systems comprising rSOC units can be classified into two large categories, depending on the involved chemical species: co-electrolysis or steam electrolysis.

Systems belonging to the first group usually achieve higher roundtrip efficiencies, thanks to the enhanced thermal integration deriving from reactions that involve carbon-containing species. In the context of zero CO_2 emissions, they operate as closed systems where reactants and products are stored in tanks and the exchange of chemical species with other systems is limited or non-existent. In 2011, Bierschenk et al. [8] proposed a reaction chemistry that promotes CH_4 formation inside the rSOC, thus reducing the endothermicity of the reaction and enabling exothermic electrolysis at lower operating voltages. Based on this concept, Wendel et al. [9] designed an rSOC system where methanation is promoted inside the reactor, operated at 20 bar and 680 °C. This enables an efficient exothermic operation of the stack, thus avoiding the need for a thermal energy storage (TES) unit. The same authors explored a similar system operated at atmospheric pressure, where they compared the system roundtrip efficiency with different storage alternatives for water/steam [10]. On the other hand, Mottaghizadeh et al. [11] proposed an rSOC system based on a phase-change material (PCM) for high-temperature thermal energy storage. In fuel cell (FC) mode, the rSOC works at a higher temperature than in electrolysis (EC) mode (850 °C versus 800 °C), allowing for thermal integration at higher temperature and enabling endothermic electrolysis. Reznicek et al. [12] developed a system at intermediate temperature (600 °C) and atmospheric pressure, where they analyzed the partial-load operation of the system. They showed that it can operate as low as 15 % of the rated capacity with limited roundtrip efficiency penalties: the reaction chemistry based on carbonaceous reactants permits an exothermic electrolysis even at reduced current densities. Finally, Santhanam et al. [13] proposed a similar system to that studied by Mottaghizadeh et al. [11], which can alternatively withdraw natural gas from and inject synthetic methane into the gas grid, while Lonis et al. [14] designed an rSOC system fed with methanol in FC mode, and that in EC mode produces hydrogen to be fed to a dedicated methanol production section. Table 1 gathers the main characteristics and performance parameters of the above-mentioned studies, with a focus on the rSOC operating conditions and the thermal integration solutions.

Recently, despite their intrinsic lower roundtrip efficiency, systems relying on a reaction chemistry based exclusively on steam and hydrogen have been studied as well. In order to be thermally self-sufficient, these systems necessarily require a TES unit or external supply to provide the heat for water evaporation in electrolysis mode. In addition, to sustain the endothermic electrolysis, external heaters are employed, or the operation at high voltage (above the typical thermoneutral voltage of 1.29 V for steam electrolysis) is pursued, with negative consequences on the roundtrip electrical efficiency. However, these systems are simpler and can be integrated more easily in the energy infrastructure, since they exchange with other systems only water and hydrogen and there is no CO_2 involved in the processes. Frank et al. [15] designed an rSOC system based on steam electrolysis, which is asymmetrical with respect to the operating current density (higher in electrolysis mode with respect to the fuel cell mode). The system is not coupled with a thermal energy storage unit and the electrolysis is endothermic at the design point: this requires external heat sources, both at low and high temperature, with a large impact on the system roundtrip efficiency. Perna et al. [16] designed an rSOC system based on steam electrolysis with two distinct balance-of-plant (BoP) sections for the SOFC and SOEC modes. The system is coupled with a thermal energy storage based on diathermic oil, which recovers the excess heat in fuel cell mode and delivers it in electrolysis mode for water evaporation. A similar system was studied by Wang et al. [17], focusing on the effects of

Table 1
Main characteristics and performance parameters of rSOC systems fed with carbonaceous reactant. Within the system scope, P2P (Power-to-Power) refers to the use for electricity storage. Within current density, *symmetric* refers to systems operating with identical current density in fuel cell and electrolysis mode in the respective nominal points. Within thermal energy storage (TES) types, PCM stands for phase-change material.

	Reference	[9]	[10]	[11]	[12]	[13]	[14]
	System scope	P2P	P2P	P2P	P2P	P2P	P2P / Methanol production
rSOC operating conditions	Fuel	Syngas	Syngas	Syngas	Syngas	CH_4	Methanol
	Pressure	20 bar	1 bar	25 bar	1.1 bar	25 bar	1 bar
	Cell temperature	650 °C	600 °C	850/800 °C (FC/EC)	600 °C	845/800 °C (FC/EC)	850 °C
	EC/FC power ratio*	1.37	1.25	1.65	1.3	1.61	2.7
	Current density	0.70 A/cm^2 (symmetric)	0.20 A/cm^2 (symmetric)	0.25 A/cm^2 (symmetric)	0.35 A/cm^2 (symmetric)	0.25 A/cm^2 (symmetric)	N/A
	Voltage in FC mode	N/A	0.94 V	0.74 V	0.89 V	0.77 V	N/A
	Voltage in EC mode	N/A	1.12 V	1.23 V	1.17 V	1.24 V	N/A
Performances	Stack roundtrip efficiency	72.8 %	79.9 %	60.5 %	76.0 %	62.2 %	37.5 %
	System roundtrip electric efficiency	72.6 %	68.3 %	60.4 %	53.4 %	52.9 %	36.2 %
Thermal integration	TES type	None	None	PCM	None	PCM	PCM
	TES temperature	–	–	850 and 750 °C	–	850 and 750 °C	120 °C
	Other	Internal methanation	Internal methanation	External methanation	Internal methanation	External methanation / Reforming	Methanol distillation column

* Referred to the stack power (DC) at nominal load.

the air excess ratio and the utilization factor on the stack temperature gradients and on the system roundtrip efficiency. Giap et al., on the other hand, studied two rSOC systems fed with steam from upstream processes. In their first work [18], the system does not include thermal energy storage, while in the second [19] it is coupled with metal hydrides, which serve both as hydrogen storage and as low-temperature heat source/sink. Amladi et al. [20] studied a rSOC system coupled to an ammonia synthesis process: the produced hydrogen is used as a feedstock for the Haber-Bosch reactor, while waste heat from the reactor is used as heat source for the steam generation. Table 2 collects the main characteristics of the described hydrogen-fed rSOC systems. Differently from the previous set of systems, it is visible how these rely strongly on the presence of either a TES unit or an external thermal input, such as electricity or waste heat from other processes.

In addition to the theoretical studies, specific projects addressed the experimentation of the rSOC concept. For example, Fuel Cell Energy has experimentally investigated an rSOC module of 3 kW / 15 kW (FC / EC) capacity [21]. The module was tested in a furnace environment for about a week with a day/night cycling, showing negligible degradation and a roundtrip system efficiency of 44.8 %. They plan to expand the capacity of the system to the MW-scale, and preliminary analyses on the system concept showed a predicted roundtrip efficiency of 67 %. This can be obtained by employing a low current density in FC mode (around 0.2 A/cm^2) and by optimizing the BoP (e.g., by using hydrogen expanders to reduce the parasitic consumption).

All the abovementioned works focused on the rSOC system design, and in some cases they developed parametric analyses that helped understanding the impact of operating parameters on the roundtrip system efficiency. Apart from the work of Reznicek et al. [12], where they also studied the partial-load operation of the rSOC system based on methanation, there is a lack of studies investigating the off-design operation of rSOC systems. Focusing on systems relying on steam electrolysis, different strategies are needed to allow a wide operating window spanning from the exothermic to the endothermic regime. While there is large agreement on SOFC systems off-design regulating strategies, there is limited literature regarding the investigation of the partial-load

Table 2
Main characteristics and performance parameters of rSOC system fed with hydrogen and steam. Within the system scope, P2P (Power-to-Power) refers to the use for electricity storage, while CHP (Combined heat and power) indicates uses for electricity and heat supply to a final user. Within current density, *symmetric* refers to systems operating with identical current density in fuel cell and electrolysis mode in their respective nominal points.

	Reference	[15]	[16]	[17]	[18]	[19]	[20]
	System scope	P2P	P2P + CHP	P2P	P2P	P2P	Ammonia synthesis
rSOC operating conditions	Fuel	H_2	H_2	H_2	H_2	H_2	H_2
	Pressure	1 bar	1 bar	1 bar	1.1 bar	1.1 bar	1.5–10 bar
	Cell temperature	750 °C	750 °C	850 °C	750 °C	750 °C	650–800 °C
	EC/FC power ratio*	2	1.6	1.39	1.51	N/A	N/A
	Current density	0.50 A/cm^2 (FC) - 0.80 A/cm^2 (EC)	0.44 A/cm^2 (symmetric)	0.68 A/cm^2 (symmetric)	0.67 A/cm^2 (symmetric)	0.45 A/cm^2 (symmetric)	0.25–1.00 A/cm^2 (symmetric)
	Voltage in FC mode	0.93 V	0.81 V	0.80 V	N/A	N/A	N/A
	Voltage in EC mode	1.19 V	1.29 V	1.11 V	N/A	N/A	N/A
Performances	Stack roundtrip electric efficiency	78.2 %	62.7 %	72.5 %	N/A	N/A	N/A
	System roundtrip efficiency	51.0 %	60.0 %	58.3 %	53.8 %	47.4 %	56.7–60.3 %
Thermal integration	TES type	None	Diathermic oil	Diathermic oil	None	Metal hydride	None
	TES temperature	–	30–380 °C	27–180 °C	–	20–277 °C	–
	External input	Electricity	–	Electricity	Waste steam	Waste steam	Ammonia synthesis waste heat

* Referred to the stack power (DC) at nominal load.

operation of SOEC modules or systems [22,23]. In particular, limited effort has been dedicated to understanding the main efficiency losses at different load levels. Designing rSOC systems and choosing operating strategies that allow for a wide and efficient modulation of the generated/required electric power in both modes is key for these systems to be coupled with intermittent and highly fluctuating energy sources like wind and solar.

1.2. Scope and structure of the work

This work has been developed within the Italian public-funded Research Project of Relevant National Interest (PRIN) titled 'High Efficiency Reversible technologies in fully renewable Multi-Energy System' (HERMES). In this work, an rSOC system based on steam electrolysis and hydrogen as a fuel is designed and its operation is investigated across the wider operating window. The system has a unified balance of plant for both fuel cell and electrolysis modes, and it is coupled with molten salt thermal storage to ease the thermal integration between the two modalities. The design focuses on the rSOC module and the heat exchangers sizing. First, the heat exchangers are sized separately for fuel cell and electrolysis modes; after that, a feasible design for both modes is selected and tested. After presenting the main performance parameters of the system at nominal load, the proposed partial load regulating strategies are used to extract operating conditions at lower loads. A comprehensive analysis of the influence of main stack parameters (like fuel utilization, operating pressure and temperature) on the performance of the system at nominal load is out of the scope of this work, as addressed by other existing literature.

This work addresses the following research gaps identified in the literature review about rSOC systems:

- The partial load of a hydrogen/steam-based rSOC system with the same balance-of-plant components in the two modes is studied. To the authors knowledge, a similar analysis has been conducted only for an rSOC system based on methanation [12], where the endothermic region of the electrolysis mode is not present.
- Available works dealing with hydrogen/steam operation have only addressed the performances of rSOC or SOEC systems at various current densities to mimic their partial-load behavior without a fixed sizing of the auxiliary systems. Moreover, to enable the endothermic electrolysis they assumed to provide the required high-temperature heat only by means of external electrical heating. As a novel aspect of this work, electric heaters and hydrogen-fed combustors placed before or after the stack are compared, and their effects on the system efficiency throughout the whole operating window is investigated.
- The analysis of the partial load looks in detail at the BoP consumption and how it affects the system efficiency at different system power levels. In this regard, equations that describe the efficiency losses with respect to the stack efficiency in both modalities are defined for this purpose for the first time. These can describe the efficiency losses based on either additional electricity consumption from the BoP or hydrogen loss from burners or purging.
- Many works in the literature, as shown above, have studied how a thermal storage can be coupled to the system. Nevertheless, none of them have investigated the trend of the recovered/required thermal power at various load. Both the system efficiency and the thermal power generation/consumption maps can be useful for further analyses to describe the interaction of the rSOC system with storage units, variable-load end-use demands, and energy sources when simulated over long time windows.

A preliminary version of the system has been described in a previous work [24], where simplified assumptions for the off-design behavior of the heat exchangers and the BoP were made during the modelling phase. In this work, these assumptions are reviewed to properly assess the performances of the system at operating points different that the nominal one.

2. System description

This section illustrates the plant layout and the functioning mechanism of the system in the two modalities at nominal load. After that, the strategies for the partial load operation of the system in both modalities are presented.

2.1. Plant layout

The system layout is depicted in Fig. 1 in its two functioning modalities. Here, its main features are reviewed and the four different configurations that enable a wide partial load operation of the system in EC mode are presented.

The rSOC operates at ambient pressure and at 750 °C in both modalities. The system features one balance of plant for both modalities and the presence of a thermal energy storage at intermediate temperature (270 °C - 480 °C). The thermal energy storage is based on molten salt composed of a mixture of sodium nitrate ($NaNO_3$–60 $\%_{wt}$) and potassium nitrate (KNO_3–40 $\%_{wt}$). This heat transfer medium, otherwise known as *solar salt*, is chosen due to its already wide usage in commercial concentrating solar power (CSP) applications [25]. The configuration of the heat exchangers is bounded by the assumed hot and cold temperature of the molten salt, and by the necessity to bring the reactants to the rSOC operating temperature. In fuel cell mode (FC), thermal power can be extracted from the air exhaust and stored in the molten salt thermal storage. In electrolysis mode (EC), the stack is operated with a current density high enough that the reaction is exothermic, and thermal power can be extracted for the air exhaust flow as well. In this way, at nominal load, the only thermal input to the system is that required for water evaporation, which is provided by the hot molten salt stored during FC mode and partially during EC mode as well. The heat recovery occurs along the air side, which works in the same way in both modalities: ambient air is preheated at the expenses of the air exhaust in two regenerative heat exchangers (HX-AIRPR and HX-A-HT), while the heat recovery occurs in the air-to-molten salt heat exchanger (HX-S-AIR).

Regarding the fuel side, in fuel cell mode, the input is hydrogen from the storage, which is mixed with recirculated hydrogen from the exhaust. This is pre-heated in a single regenerative heat exchanger (HX-F-HT) and then sent to the rSOC module. A mixture of steam and hydrogen exits the rSOC, cools down in HX-F-HT and then it is sent to the condenser, where water is removed. A small purge flow is considered to prevent the build-up of contaminants in the system. In electrolysis mode, the input to the fuel side is liquid water. Water is brought close to 100 °C in a low-temperature pre-heater (HX-FUEPR) at the expense of the fuel exhaust, and then sent to the fuel-side molten salt heat exchanger (HX-S-FUEL), where it is evaporated and slightly superheated. To avoid water evaporation at any time in the pre-heater, the possibility to partly bypass it on the exhaust side is given, as shown by the dashed line. After water evaporation, the recirculated hydrogen is admixed to form a mixture of 90–10 %vol. of steam-H_2. A slightly reducing mixture at the stack inlet is commonly advised as it helps in preventing the electrode oxidation [26]. The final step of preheating is completed in HX-F-HT and the mixture is fed to the stack. The exhaust mixture cools down in the regenerative heat exchangers and it is sent to the condenser, where water is removed. Hydrogen is exported and a small fraction is recirculated. Depending on the current density and voltage, endothermic electrolysis may occur. For this reason, the system is equipped with fuel and air heaters to manipulate the inlet flows temperature, as discussed later.

2.2. Nominal and partial load regulating strategies

The definition of the nominal and partial load regulating strategy for the rSOC system derives from control strategies of stand-alone SOFC and

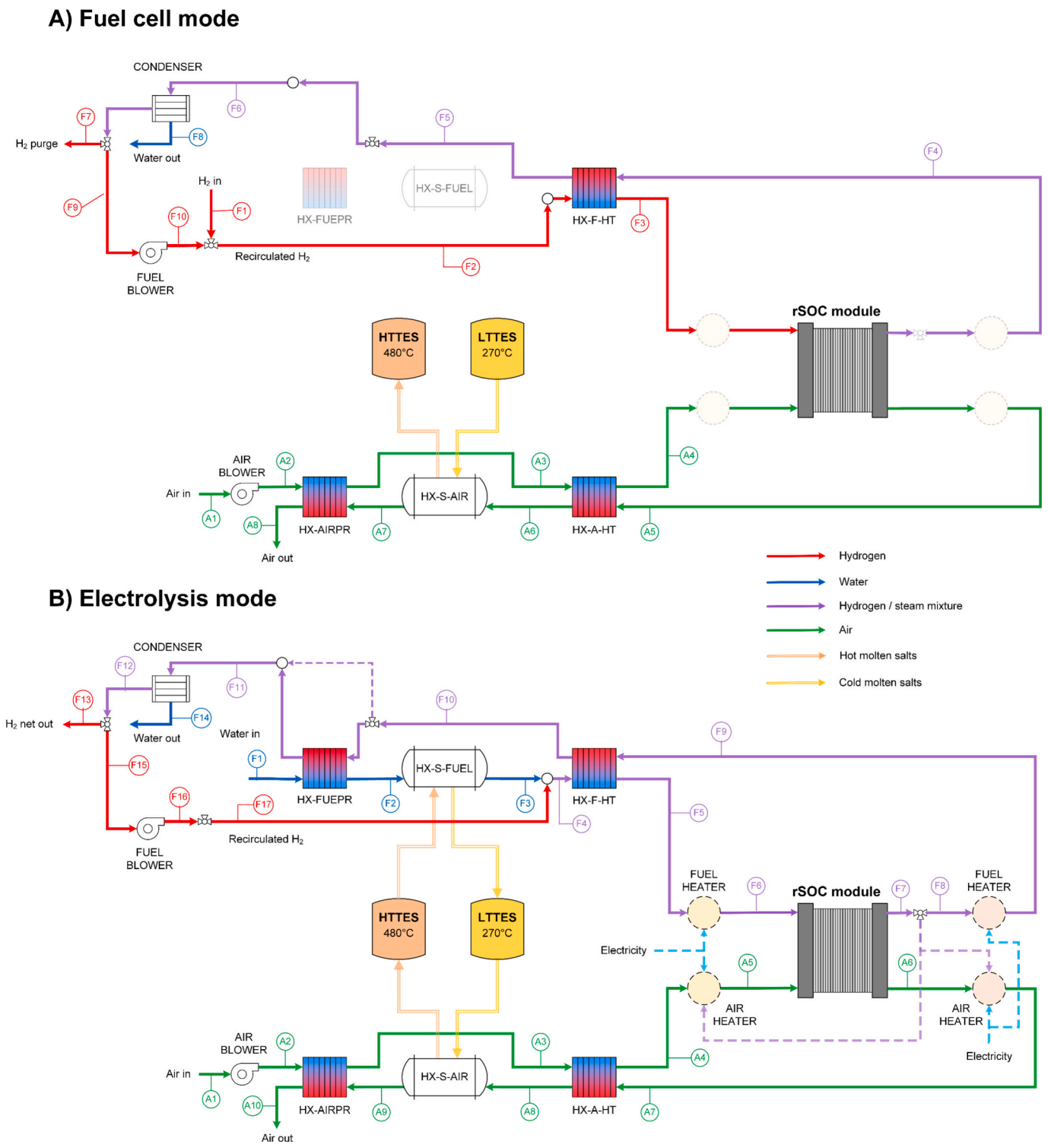

Fig. 1. Plant layout of the rSOC system, with active flows in the SOFC (A) and SOEC (B) modality. The four different plant configurations allowing the partial load operation are shown altogether for both modalities with the dashed arrows, but they are analyzed separately. Fuel-side heaters are always powered by electricity, whereas air-side heaters can be either electric heaters or hydrogen-fed combustors.

SOEC systems. Established control strategies for SOFC systems include: (1) manipulation of the current density to reduce or increase the system power generation; (2) manipulation of the fuel flow to maintain constant fuel utilization; (3) manipulation of the system balance of plant to maintain the inlet fuel cell temperature [27–30], and (4) limit the in-out temperature difference in the stack to 100 °C [31,32]. When dealing with SOEC systems, the available literature on the topic is scarcer. In this case, the regulating strategy should consider the transition from exothermic to endothermic behavior, and vice versa. Therefore, the control with air mass flow rate on its own is not enough. Petipas et al. studied the part-load regulation in a limited range around the thermo-neutral voltage by only manipulating the current density and without using sweep flows to extract the produced oxygen on the anode side [33]. In a subsequent work, they proposed to extend the operating range

throughout the endothermic region by introducing electric heaters and by varying the air sweep mass flow rate [23]. On the other hand, Sanz-Bermejo et al. proposed different regulating strategies that allow for a wide operating window, either by keeping the cell at fixed temperature or voltage [22]. In the former, electric heaters were employed to keep a constant cell inlet temperature in exothermic and endothermic regions. In the second strategy, the cell temperature was varied to maintain the reaction always at the thermoneutral point.

The partial load strategy employed for this work derives from the above-mentioned strategies, while considering technical operating limits for the air blower. A sweep flow of air is always maintained and varied in both exothermic and endothermic regions due to safety reasons. Moreover, a constant utilization factor on the fuel side is considered in both modalities. Especially in electrolysis mode, it allows large savings in the required heat for evaporation at lower loads. Finally, keeping a fixed cell temperature is critical for allowing fast transitions while limiting excessive temporal thermal gradients at the cell level [34–37].

Therefore, the proposed regulating strategy differs depending on the operating modality (FC or EC), and whether the electrolysis is exothermic or endothermic.

In fuel cell mode:

- The air flow rate is regulated to extract the generated heat within the stack, while respecting the limit of 100 °C temperature difference between inlet and outlet.
- Multiple variable-speed fans placed in parallel are used to handle the large variations in mass flow rate at different power levels.

In electrolysis mode:

- Exothermic region (*Strategy A*): the same strategy used for the fuel cell mode applies.
- Transition to endothermic region (*Strategy B*): as the heat generation reduces and the thermoneutral point is approached, the minimum allowable air mass flow rate that can be processed by the fans is reached. At this point, the air mass flow is fixed and the high-temperature heaters are activated to maintain the stack temperature: a further decrease in heat generation with fixed air flow rate would lead to unwanted cooling of the stack. As the operation becomes fully endothermic, the same strategy is applied until the maximum temperature difference of 100° is reached across the stack (corresponding to the point where a temperature of 850 °C is reached at the cell inlet, if the outlet temperature is kept constant to the design value of 750 °C).
- Endothermic region (*Strategy C)*: the high-temperature heaters are regulated to keep an inlet temperature to the cell of 850 °C, while the air mass flow rate is regulated to provide the required heat by the reaction.

In scientific works dealing with high-temperature solid oxide cell systems, the use of electric heaters placed at inlet of the stack is the common choice to regulate the stack temperature. In this work, different configurations to provide heat to the air side are explored: an electrical resistance heater and a hydrogen-fed combustor. In particular, the latter can be fed with a fraction of the hydrogen-rich exhaust fuel stream, thus decreasing the net hydrogen generation of the system, but saving electricity consumption at the BoP level. The impact on the system efficiency of the two options is discussed in the results section. Moreover, the additional heater can be placed before the stack, directly increasing the air inlet temperature, or after the stack, increasing the air exhaust temperature which in turn increases the air inlet temperature in HX-A-HT. The combination of these alternatives produces a set of four configurations, summarized in Table 3, and shown in Fig. 1.

Table 3
Four different configurations to enable proper thermal integration at partial load.

Configuration	Description
Pre-EH	Electric pre-heater
Pre-HC	Pre-combustor fed with hydrogen-rich fuel exhaust
Post-EH	Electric post-heater
Post-HC	Post-combustor fed with hydrogen-rich fuel exhaust

3. System modelling

The model of the rSOC system is developed in Aspen Plus® V11. In this section, the methodology and assumptions for the main components of the system, namely the rSOC module, the heat exchangers, and the fans are described. This section also defines performance indicators that will be used in the analysis of the results, like stack and system efficiency, roundtrip efficiency, and system efficiency losses.

3.1. rSOC stack and module

In the literature, models for numerical simulation of systems based on reversible solid oxide cells have been presented with different levels of details (from stack to whole system) and validated according to experimental results. When dealing with the entire system, the preferred choice is to use zero-dimensional models due to their simplicity and ability to produce fast but reliable results [11,15,18]. On the other hand, more detailed models are sometimes adopted to capture complex dynamics and detailed spatial gradients within the stack [37]. This work focuses on the system performance analysis at various loads with a steady-state approach, thus the preferred choice for the rSOC model is to employ a zero-dimensional component. The impact of operating points on the mass and energy flows exchanged by the stack are adequately represented, while internal stack design is out of the scope (and in general strictly related to confidential development of the manufacturer).

Despite a dedicated component modelling electrochemical devices is not included in Aspen Plus libraries, a combination of a reactor and a separator is suitable to reproduce the component behavior, and it is the common approach presented in literature. The calculation of electrochemical parameters linking reaction development and electricity consumption/generation is integrated according to the direct relation between mass flow rate and current as well as the current-voltage relation (polarization curve). A stoichiometric reactor (RStoich) is employed, given that the reaction stoichiometry is known ($H_2 + ½\ O2 \leftrightarrow H_2O$). Downstream, the products of the reaction are fed to a separator, which splits the mixture of steam and hydrogen from that of nitrogen and oxygen, assuming that the electrolyte is perfectly impermeable to gaseous species. The net heat duty of the reactor is extracted (or provided) via two energy streams: the electrical power absorbed/generated by the electrochemical reaction and the heat exchange between the stack and the environment. The latter is always set to zero via air mass flow rate regulation and/or inlet gas temperature manipulation, such that the net heat duty of the reactor coincides with the electricity output to the stack and the generated/requested heat of the reaction is provided/extracted by increasing or decreasing the gases temperature.

The magnitude and direction of the electric power generation or consumption of the rSOC module is an input to the model. Via a Fortran calculator, the electrochemical behavior of the stack is solved, according to the stack geometry (cell surface area, number of cells), the electrochemical characteristics of the cell (see below), and the operating conditions (mostly the utilization factors, U_f). Starting from the value of the electric power generation/consumption of the stack, the calculator computes the current density (j) and the cell operating voltage (V). From the utilization factor, it also computes the inlet flow rate of hydrogen or steam to be fed to the reactor.

In the relevant range of operation (i.e., at current density beyond the condition of predominant activation loss and sufficiently lower than entering the condition of concentration losses), the electrochemical behavior of a solid oxide cell exhibit a linear behavior [38–40]. Hence, the polarization curve is described with good accuracy by the values of the open-circuit voltage (OCV) and the area-specific resistance (ASR):

$$V = OCV - j \cdot ASR \quad (1)$$

where the current density j is positive in fuel cell mode and negative in electrolysis mode.

Data for OCV and ASR adopted in this work for the FC and EC modes are extracted from the experimental results by Barelli et al. [39]. They investigated the reversible operation of a short stack of planar commercial anode-supported solid oxide cells (manufactured by SolydEra [41]), operated at 750 °C. Table 4 reports the assumptions used in this work for the rSOC model. Given the lack of an experimental curve with the exact inlet composition assumed in FC mode (98 $\%_{mol}$ H_2), the closest condition is used for input data (90 $\%_{mol}$ H_2 feed). The modelled linear polarization curves are compared to the experimental curves in the *Supplementary Materials*, showing limited differences in both FC and EC modes (<2 %).

The rSOC module is designed to have a 3:1 power capacity ratio between electrolysis and fuel cell mode, generating 1 MW_e of electrical power when running at nominal load in FC mode. Based on expected improvements in solid oxide cells manufacturing, a cell active area of 400 cm^2 is considered, which is equivalent to a cell with an edge length of 20 cm [38]. In both modes of operation, the reaction is assumed to have a fuel utilization factor of 0.70. To determine the appropriate number of cells of the rSOC module, a nominal current density of 0.5 A/cm^2 has been considered for the FC mode. This value of current density requires 6630 cells to reach the design power production of 1 MW_e. Given the total number of cells, a configuration consisting of 22 stacks made of 300 cells each can be assumed as reasonable, considering expected sizes of industrial rSOC modules. Therefore, the rSOC module has been considered as a unitary structure without further sub-units, ultimately assuming that all stacks are always operated simultaneously with the same value of current density. In electrolysis mode, on the other hand, this number of cells entails a current density of 0.81 A/cm^2 to meet the requirement of 3 MW_e, which is in line with short-term expected development [42]. The resulting operating voltage in EC mode at nominal load is equal to 1.39 V, corresponding to a fully exothermic operation at nominal load.

Table 4
Sizing features and assumptions for the rSOC module modelling.

Parameter	FC mode	EC mode	Notes
rSOC module nominal power ($kW_{el,DC}$)	1000	3000	Own assumption
Cell active area (cm^2)	400		[38]
Total number of cells	6630		Preliminary design
Operating temperature (°C)	750		[39]
Operating pressure (bar)	1.1		[39]
ASR (Ω cm^2)*	0.588	0.657	[39]
OCV (V)*	1.049	0.860	[39]
Nominal current density (A/cm^2)	0.500	0.812	Own assumption / Preliminary design
Nominal cell voltage (V)	0.755	1.393	Preliminary design
Oxygen electrode inlet molar composition (O_2 / N_2)	0.21 / 0.79		Air inlet
Fuel electrode inlet molar composition (H_2 / H_2O)	0.98 / 0.02	0.10 / 0.90	Own assumption
Utilization factor	0.70		[39]
Maximum temperature increase across rSOC module (°C)	100		[31,32]
Design rSOC module pressure drop (kPa)	1		Own assumption

* The ASR and the OCV values represent the operation of a short stack of six cells operated with 90/10 H_2/H_2O molar composition in FC mode, and 10/90 H_2/H_2O molar composition in EC mode.

3.2. Heat exchangers

The heat exchangers are modelled as countercurrent lumped components. The sizing procedure aims at finding the design UA product given specific design specifications. The sizing is performed separately for the FC and EC modes, and then for each heat exchanger the larger UA is selected. The variation of UA in off-design conditions takes into account mass flow rates variation, type of heat exchanger, and possible fluid properties variation. At this stage of the analysis, a detailed geometric design for each heat exchanger is not considered. Nevertheless, general considerations on the type of heat exchanger can be proposed, which help in design procedure and off-design modelling. Air preheaters are considered to be countercurrent plate heat exchangers. The same can be applied to the low-temperature pre-heater and high-temperature pre-heater on the fuel side. The molten salt evaporator on the fuel side choice derives from CSP application and could take different forms. For the purpose of this work, the U-tube molten salt steam generator studied by Zou et al. [43] is taken as reference, since it can handle both water evaporation at and superheating in one component. The air-to-molten salt heat exchanger, on the other hand, can be considered to be a shell-and-tube heat exchanger where the molten salt flows inside the tubes.

3.2.1. Sizing procedure

In this section, the main assumptions on the design specifications of each heat exchanger are addressed.

The heat exchanger of the air side operates very similarly in the two modalities, except for the different thermal capacities of the inlet and exhaust flows between the two modalities: in fuel cell mode, the air exhaust has a lower thermal capacity due to the transfer of oxygen ions to the fuel side, while the opposite occurs in electrolysis mode. For this reason, an approach temperature difference specification has been used for the low-temperature pre-heater on the cold side and the hot side for the FC and EC modes, respectively. In addition, the main constraints to look at when properly designing the heat exchanger network on the air side are the heat recovery towards the molten salt and the in-out temperature difference across the rSOC module. To allow the heat recovery along the air side, the air inlet temperature to the molten salt heat exchanger must be sufficiently higher than 480 °C in both modalities. Once the design specifications for the low-temperature and high-temperature recuperators are set, the control on the in-out temperature difference of the rSOC module can be pursued by properly designing the air-to-molten salt heat exchanger. In particular, a hot air outlet temperature is given as design specification.

The heat exchangers of the fuel side are the low-temperature pre-heater and the steam generator in electrolysis mode, and the high-temperature pre-heater in both modalities. As for the latter, the method of the approach temperature difference is used for both modes. Regarding the low-temperature pre-heater, this is sized such that the cold stream exists in slightly sub-cooled conditions. The molten salt steam generator, on the other hand, is sized by imposing a steam outlet temperature. Table 5 summarizes the design specification and motivations of each heat exchanger in both modalities.

3.2.2. Off-design

When dealing with the off-design behavior of heat exchangers that are modelled as lumped components, the UA variation in working points that are far from the design one can be expressed as a function of the hot and cold mass flow rates variation, as previously done in Refs. [44–47]. Assuming to express the specific heat transfer coefficients variation as a function of the Reynolds number elevated to an exponent n, while assuming constant fluid properties (and thus constant Prandtl number), the following relation can be used:

Table 5
Design specification for the heat exchangers in fuel cell and electrolysis mode.

	Heat exchanger	Design specification	Motivation
FC mode	HX-AIRPR	ΔT hot outlet / cold inlet = 20 °C	Different thermal capacity of the flows
	HX-S-AIR	Hot outlet = 455 °C	Control on the stack temperature difference
	HX-A-HT	Hot outlet = 530 °C	Margin on hot molten salt temperature
	HX-FUEPR	*Bypassed*	
	HX-S-FUEL	*Bypassed*	
	HX-F-HT	ΔT hot inlet / cold outlet = 20 °C	Different thermal capacity of the flows
EC mode	HX-AIRPR	ΔT hot inlet / cold outlet = 20 °C	Different thermal capacity of the flows
	HX-S-AIR	Hot outlet = 455 °C	Control on the stack temperature difference
	HX-A-HT	Hot outlet = 530 °C	Margin on hot molten salt temperature
	HX-FUEPR	Cold outlet = 90 °C	Sub-cooled liquid entering HX-S-FUEL
	HX-S-FUEL	Hot outlet temperature = 300 °C	Arbitrary choice
	HX-F-HT	ΔT hot outlet – cold inlet = 20 °C	Different thermal capacity of the flows

$$\frac{UA_{off}}{UA_{des}} = \frac{\dot{m}_{h,des}^{-n} + \dot{m}_{c,des}^{-n}}{\dot{m}_{h,off}^{-n} + \dot{m}_{c,off}^{-n}} \quad (2)$$

where the subscripts *des* and *off* are used for parameters in design and off-design conditions, respectively, while *c* and *h* refer to the cold and hot sides of the heat exchangers, respectively. Eq. (2) is applied to all heat exchangers that deal with the same fluid in both modalities, such as those on the air side, and those used for liquid water preheating and steam generation. A simplification can be applied to the evaporator, where the cold side is characterized by a much larger heat transfer coefficient, and the UA variation can be expressed as a function of the hot side mass flow variation only. It can be reasonably assumed that, when the load of the rSOC module is reduced while keeping a constant utilization factor, the composition of the exhaust gases is nearly constant, and thus the fluid properties. An exception lies in the high-temperature recuperative heat exchanger on the fuel side, which not only experiences a considerable variation in mass flow rate in the two modalities, but also sees a dramatic change in composition. In particular, on the cold side, slightly humidified hydrogen is present in FC mode, while a mixture of 90/10 H_2O/H_2 in EC mode. On the hot side, a water-hydrogen mixture is present, mostly composed of steam in FC mode and mostly of hydrogen in EC mode. In this regard, Eq. (3) and Eq. (4) can be used, according to Ref. [45], to account for variations in the Prandtl number as well, and in particular to changes in the specific heat capacity (c_p), thermal conductivity (k), and dynamic viscosity (μ) of the streams:

$$\frac{UA_{off}}{UA_{des}} = \frac{\beta_{h,des}^{-n} + \beta_{c,des}^{-n}}{\beta_{h,off}^{-n} + \beta_{c,off}^{-n}} \quad (3)$$

$$\beta = \dot{m}^{n} \cdot c_p^{c} \cdot k^{1-c} \cdot \mu^{c-n} \quad (4)$$

where c = 0.4 for the hot fluid and c = 0.3 for the cold fluid.

In Eqs. (3) and (4), the coefficient n depends on the correlations chosen to describe the heat transfer phenomena, and it may be different for the hot and cold sides. For example, the Dittus-Boelter correlation for internal flow in pipes is used for all those heat exchangers that have been identified as plate heat exchangers, such as the air low-temperature and high-temperature recuperators on the air side, the liquid water preheater and the high-temperature recuperator on the fuel side. In these cases, an exponent $n = 0.8$ is used for both hot and cold sides. In heat exchangers where the molten salt is involved, the Dittus-Boelter correlation is used for fluids inside tubes, while for fluids outside tubes the Zukauskas correlation that is valid for external flow on tube bundles is used as a first approximation, with exponent $n = 0.63$ [48].

Pressure drops across heat exchangers are assumed to be equal to 2 % of the inlet flow pressure, and in off-design they are scaled proportionally to the square of the mass flow rate.

3.3. Air fans and fuel blowers

The proposed system operates at atmospheric pressure. Therefore, blowers that provide a limited prevalence to the fluids are sufficient to overcome the pressure drops in the heat exchangers and the rSOC module.

Given the large variations in air mass flow rates that the system experiences when working over wide operating windows and in the two modalities, variable-speed fans are deemed appropriate. They can easily regulate the required mass flow rate while granting large savings in electricity consumption at lower loads. General affinity fan laws are used to model the head and the power consumption as functions of the processed volumetric flow rate. According to these, the pressure increase and the mechanical power of the fans are proportional to the square and to the cube of the processed volumetric flow rate, respectively. The isentropic and mechanical efficiencies are set as constants and equal to 85 % and 95 %, respectively [49]. The combined efficiency of the electric motor and of the variable-frequency drive (VFD) spans from nearly 90 % at nominal load down to about 58 % at minimum load [50]. For the analysis, a second-order polynomial interpolation is used. According to the operating maps of commercial industrial-size centrifugal fans [49], a value of 30 % of the rated mass flow rate is considered as minimum load. Given this limitation, one single fan may not be adequate to handle the expected large variations in air mass flow rate in the system. Hence, multiple identical fans are used in parallel, each sized to handle a fraction of the maximum air mass flow required by the system, which corresponds to the nominal operation in FC mode. At any operating condition, the required air mass flow rate is split evenly among the active fans, hence resulting in the same pressure increase. One or more fans are turned off when they reach their minimum technical limit.

Regarding the fuel blowers, preliminary simulations have shown that their consumption is negligible with respect to those of other BoP components, especially the air fans. Therefore, a simplified approach is followed for these components. The fuel blower in both modalities is set to provide enough pressure increase to mix the recirculated hydrogen to the main feed, either hydrogen or steam. For any point of the partial load, their pressure increase is set constant to the nominal one.

3.4. Other balance of plant components

The assumptions used to model the remaining balance-of-plant components are gathered in Table 6. The pump for water circulation in the electrolysis mode operation is excluded from the modelling, since preliminary calculations showed that its consumption is negligible with respect to other BoP components. The implementation of the molten salt thermal storage in the model focuses on the heat exchangers only, being the tank sizing dependent on the specific context where the rSOC system is employed. The flow rate of molten salts is calculated for each operating point in order to obtain the given temperature difference between the two tanks. The condenser for heat rejection and water separation is represented by the electrical consumption for its auxiliary components, assumed equal to 0.8 % of the rejected power, based on estimates on similar systems [51]. The downstream hydrogen compression is not

Table 6
Assumptions for the balance-of-plant components modelling, system boundaries, and pressure drops across the system.

Parameter	Value
Feedwater inlet temperature (°C)	25
Hydrogen inlet temperature (°C)	25
TES hot tank temperature (°C)	480
TES cold tank temperature (°C)	270
Heat exchangers design pressure drop (%)	2
Air/Fuel blower isentropic efficiency (%)	85
Air/Fuel blower mechanical efficiency (%)	95
Auxiliary electricity consumption for heat rejection (% of rejected power)	0.8
Condenser temperature (°C)	40
Electric heater efficiency (%)	99
Combustor thermal losses (%)	1
Electric heaters/combustors design pressure drop (%)	2
Inverter/Rectifier efficiency (%)	95

considered at this stage of the analysis, as highly specific on the specific end use or storage option. The table also summarizes the pressure drops for heat exchangers and heaters.

3.5. Performance indicators

In this section, useful indicators to describe the performances of the system are presented. Stack and system efficiencies can be defined separately for the two modalities and used to compute the roundtrip efficiency of the stack and the overall system. Additionally, at partial load, and especially with the onset of the regulating strategy involving the additional heat provision, it becomes relevant to investigate the different mechanisms responsible for the system efficiency losses.

3.5.1. Stack and system efficiency

For the fuel cell mode, stack and system efficiencies are defined as follows:

$$\eta_{\text{stack,FC}} = \frac{P_{\text{rSOC,FC}}}{\dot{m}_{H_2,\text{cons}} \cdot \text{LHV}_{H_2}} \tag{5}$$

$$\eta_{\text{el,sys,FC}} = \frac{P_{\text{el,net}}}{\dot{m}_{H_2,\text{in}} \cdot \text{LHV}_{H_2}} \tag{6}$$

where $P_{rSOC,FC}$ is the electrical power produced by the rSOC module and $\dot{m}_{H_2,cons}$ is the mass flow rate of hydrogen consumed by the reaction in FC mode. An alternative formulation for the stack efficiency would consider the inlet hydrogen flow in the stack and the stack utilization factor to account for the actual hydrogen that is converted. In the system efficiency definition, $P_{el,net,FC}$ accounts for the losses of the inverter (according to its efficiency η_{inv}) and the BoP consumption, comprising the fuel and air blowers and the auxiliaries, as shown by Eq. (7), while $\dot{m}_{H_2,in}$ accounts for the hydrogen make-up entering the fuel side of the system (thus excluding the amount that is internally recirculated):

$$P_{\text{el,net,FC}} = P_{\text{rSOC,FC}} \cdot \eta_{\text{inv}} - \sum P_{\text{aux,FC}} \tag{7}$$

In electrolysis mode, the definitions are the following:

$$\eta_{\text{stack,EC}} = \frac{\dot{m}_{H_2,\text{prod}} \cdot \text{LHV}_{H_2}}{P_{\text{rSOC,EC}}} \tag{8}$$

$$\eta_{\text{el,sys,EC}} = \frac{\dot{m}_{H_2,\text{out}} \cdot \text{LHV}_{H_2}}{P_{\text{el,tot}}} \tag{9}$$

where $P_{rSOC,EC}$ is the electrical power consumed by the module, $\dot{m}_{H_2,prod}$ is the total hydrogen produced by the electrochemical reaction, and $\dot{m}_{H_2,out}$ is the net hydrogen exported from the fuel branch of the system. In the system efficiency definition (Eq. (10)), $P_{el,tot,EC}$ accounts for the rectifier loss (according to its efficiency η_{rect}) and the BoP consumption, comprising the blowers, the auxiliaries and the electric resistance heater, when present.

$$P_{\text{el,tot,EC}} = \frac{P_{\text{rSOC,EC}}}{\eta_{\text{rect}}} + \sum P_{\text{aux,EC}} \tag{10}$$

Finally, a first-principle efficiency for both modalities can be defined, where the heat exchanged with the molten salt is considered. $\dot{Q}_{out}$ is the total thermal power that is recovered in FC mode, while $\dot{Q}_{in}$ is the net thermal power required for water evaporation in EC mode. In the latter case, a net input is considered, which accounts for the total input for evaporation in the water branch of the system, minus the amount that can be simultaneously recovered from the air branch.

$$\eta_{\text{I,sys,FC}} = \frac{P_{\text{el,net}} + \dot{Q}_{\text{out}}}{\dot{m}_{H_2,\text{in}} \cdot \text{LHV}_{H_2}} \tag{11}$$

$$\eta_{\text{I,sys,EC}} = \frac{\dot{m}_{H_2,\text{out}} \cdot \text{LHV}_{H_2}}{P_{\text{el,tot}} + \dot{Q}_{\text{in}}} \tag{12}$$

3.5.2. Roundtrip efficiency

The roundtrip efficiency of rSOC systems can be defined in different ways. Some of the works cited in the rSOC systems review, which investigate the performances of symmetrical systems [10–13] often use the following definitions for the stack and for the overall system, respectively:

$$\eta_{\text{RT,stack}} = \frac{P_{\text{rSOC,FC}}}{P_{\text{rSOC,EC}}} \tag{13}$$

$$\eta_{\text{RT,system}} = \frac{P_{\text{rSOC,FC}} - \sum P_{\text{aux,FC}}}{P_{\text{rSOC,EC}} + \sum P_{\text{aux,EC}}} \tag{14}$$

These definitions can be applied only when the rSOC system operates with comparable electrochemical conditions between the two modalities. In other words, when the current density is equal in magnitude between the fuel cell and the electrolysis operation. When dealing with asymmetrical systems like the one investigated here, the definitions of Eq. (13) and Eq. (14) may not be appropriate. In the specific case of this work, due to the higher current density in electrolysis mode with respect to fuel cell mode, the following and more general definitions can be used:

$$\eta_{\text{RT,stack}} = \eta_{\text{stack,FC}} \cdot \eta_{\text{stack,EC}} \tag{15}$$

$$\eta_{\text{RT,system}} = \eta_{\text{el,sys,FC}} \cdot \eta_{\text{el,sys,EC}} \tag{16}$$

3.5.3. System efficiency losses

When evaluating the performances of energy conversion systems, it is commonly beneficial to identify the main sources of losses and evaluate them in relation to the energy input to the system. This allows for the calculation of efficiency losses as compared to a unitary or reference efficiency. In the case of a rSOC system, the system efficiency in each modality can be compared to the stack efficiency of the respective modality. In this specific case, two types of major losses can be defined: those related to hydrogen or electricity consumptions. A detailed demonstration to derive the losses definitions is presented in the Appendix.

In fuel cell mode, the system losses are related only to the BoP electricity consumptions and they are defined, for each *i*-th loss term, as follows:

$$\Delta\eta_{i,el,FC} = \frac{P_{loss,i}}{\dot{m}_{H_2,in} \cdot LHV_{H_2}} \tag{17}$$

In FC mode, the term $P_{loss,i}$ is a general term for the air blower, the fuel blower, the auxiliary electrical consumption and the inverter-related loss.

In electrolysis mode, the system losses are related to *additional electricity consumptions* of the BoP, including the electric resistance heater

when present, or to *missed hydrogen exports*. The system efficiency losses related to the auxiliary consumptions in EC mode are expressed via the stack efficiency (Eq. (18)). This means that the additional electricity consumptions of the BoP could have been used to power the rSOC to produce additional hydrogen.

- *Additional electricity consumptions (EC):*

$$\Delta\eta_{i,el,EC} = \eta_{stack,EC} \cdot \frac{P_{add,i}}{P_{el,tot}} \tag{18}$$

- *Missed H_2 exports (EC):*

$$\Delta\eta_{i,H_2,EC} = \frac{\dot{m}_{H_2,loss,i} \cdot LHV_{H_2}}{P_{el,tot}} \tag{19}$$

In EC mode, the term $P_{add,i}$ is a general term for the electrical consumption of the BoP that is common with the FC mode, plus the electric heater consumption, if present, and the rectifier-related loss. The term $\dot{m}_{H2,loss,i}$ is a general term for the additional hydrogen consumption in the combustor, if present.

With such definitions of the system efficiency losses, the following relationship exists between the stack and the system efficiency, in either of the two modalities (here represented with the letter *M*):

$$\eta_{stack,M} = \eta_{el,sys,M} + \sum \Delta\eta_{i,H_2,M} + \sum \Delta\eta_{i,el,M} \tag{20}$$

4. Nominal design results

Detailed results about the heat exchangers sizing and the design stream parameters for both modalities are reported in the Supplementary Material. The selected UA for the air side heat exchangers derives from the FC mode design phase, while the UA chosen for the fuel side heat exchangers derives from the sizing performed in EC mode. Even if not optimal for each mode separately, this sizing represents a trade-off that enables the system to operate with one set of regenerative heat exchangers without issues when switching. Hereafter, the main results of the system operation at nominal load are presented for both modalities.

4.1. System performance

The main performance indicators of the system operated at nominal load are gathered in Table 7. In fuel cell mode, the system is characterized by a stack efficiency of 60.2 % and a system efficiency of 53.7 %. The reduction is mainly attributable to the large consumption of the air fans, responsible for 95 % of the BoP consumption. The highly exothermic oxidation reaction in fuel cell mode requires a large air mass flow rate to remove the generated heat inside the rSOC module. In particular, a mass flow rate of 6.1 kg/s is required at nominal conditions, leading to about 81 $kW_{el,AC}$ consumption of the fans. To allow a wide operating window in FC mode, a set of three fans placed in parallel is chosen, each of them with an operating window of 30–100 % of the nominal mass flow rate. Therefore, at nominal load, each fan process around 2 kg/s of air, providing the same pressure increase.

Table 7
Main performance parameters of the rSOC system at nominal load.

		FC mode	EC mode
rSOC module	rSOC module power ($kW_{el,DC}$)	1000	3000
Hydrogen	Mass flow rate (kg/s)	Input: 0.014	Output: 0.023
Air	Inlet mass flow rate (kg/s)	6.11	2.01
	Outlet temperature (°C)	56.5	75.2
Thermal storage exchange	Thermal power direction	Net output	Net input
	Molten salts mass flow rate (kg/s)	1.86	2.14
	Thermal power (kW_{th})	502	580
System performance	BoP consumption ($kW_{el,AC}$)	85.5	38.6
	System electric power ($kW_{el,AC}$)	894	3100
	Stack electric efficiency (%)	60.2	90.0
	System electric efficiency (%)	53.7	87.1
	First-principle efficiency	83.1	75.0 / 70.7*
	Stack electric roundtrip efficiency (%)	54.2	
	System electric roundtrip efficiency (%)	46.7	

* Assuming that heat is not recovered from the air side in EC mode.

In electrolysis mode, the system is characterized by a stack efficiency of 90.0 % and a system efficiency of 87.1 %. In this case, the limited heat generation inside the rSOC module requires a much lower air mass flow rate to be circulated into the system (2.0 kg/s instead of 6.1 kg/s in FC mode). These values translate into a stack roundtrip efficiency of 54.2 % and a system electrical roundtrip efficiency of 44.7 %. In this case, one fan is enough to process the required air flow rate. An extensive analysis on the system efficiency losses of all BoP components is performed in the partial load results section of this work. It shall be evidenced that the overall efficiency levels are of course influenced by the technological assumptions on the SOC; other analyses, employing different SOC technologies and operating at improved voltage-current setpoints may show the possibility to reach higher efficiency targets.

Despite the higher nominal current density in EC mode, the thermal power exchange with the molten salt thermal storage is comparable in the two modalities. The large air mass flow rate circulating in FC mode allows for an extensive heat recovery, while the exothermic electrolysis in EC mode helps at reducing the net thermal power requirement for water evaporation. In fact, when comparing the first-principle efficiency and the system electrical efficiency, both are largely affected by the heat recovery in all operating modes. For instance, the first-principle efficiency is equal to 83.1 % and to 75.0 % in FC and EC modes, respectively. The increase of the electrical efficiency is considerable in FC mode due to the large amount of heat that can be recovered, while the decrease in electrolysis mode is less pronounced. In EC operation, being able to simultaneously recover heat from the air side of the system is crucial to reduce the total external demand for water evaporation: in case this could not be done, the first-principle efficiency in EC mode would drop to 70.7 %.

Fig. 2 shows the overall temperature-heat (TQ) diagrams of the air side and the fuel side of the system. In each side, one of the two modalities sets the nominal condition, while in the other the gases behave as in off-design condition. In the air side, the nominal condition is set by the FC mode, which requires larger air mass flow rates due to the highly exothermic reaction and translates into larger quantities of exchanged thermal power. On the other hand, in the fuel side, the presence of large flows of water in EC mode sets the nominal condition, while the FC mode is an off-design condition, due to the extremely lower hydrogen flow rate.

On the air side, the heat exchangers are designed with two main purposes: (i) bringing the inlet cold air to the operating temperature of the rSOC module, while respecting a set temperature in-out temperature difference in the stack, and (ii) enabling the heat recovery towards the molten salts while staying above the hot tank temperature of 480 °C. When utilizing the same set of heat exchangers in EC mode, the exchanged thermal power is more than halved, but the aforementioned temperature constraints are still respected due to the decreased overall heat transfer coefficient. With respect to the total exchanged heat in the system, the fraction of heat recovery to the molten salt is equal to 11 % and 13 % in FC and EC modes, respectively. The majority of the heat is therefore required for the inlet gases pre-heating. Nevertheless, the heat recovery allows to efficiently utilize the heat generation in both modes: the temperature of the air discharged to ambient is equal to 56 °C and 75 °C, respectively.

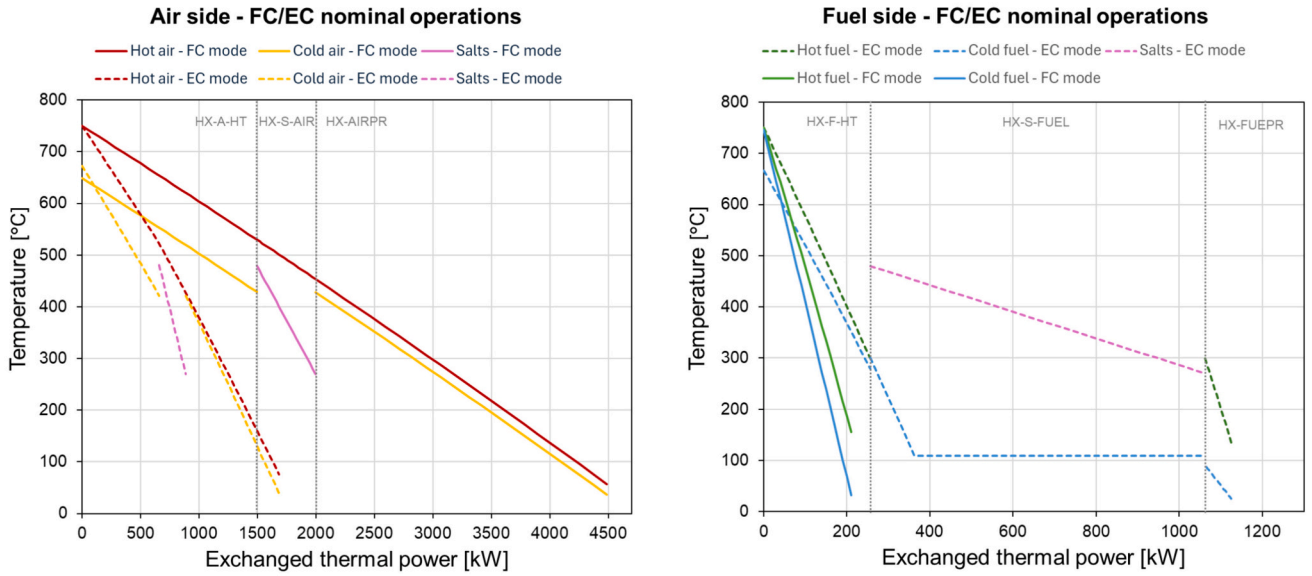

Fig. 2. Temperature-heat (TQ) diagram of the air side (left) and fuel side (right) of the system in FC and EC modes. Solid lines represent the nominal FC mode operation, while dashed lines the nominal EC mode operation. For the sake of clarity, the corresponding heat exchangers sub-sections are displayed only for the FC mode in the air side, and only for the EC mode in the fuel side.

Along the fuel side, instead, only the high-temperature heat exchanger is exploited in FC mode, since its large area is sufficient to pre-heat the cold hydrogen flow. This heat exchanger is oversized for this purpose, leading to an inlet fuel temperature close to 750 °C, in contrast to the air inlet temperature of 650 °C. Choosing an intermediate sizing for the high-temperature fuel heat exchanger could help in lowering the fuel inlet temperature. Given the extremely low fuel mass flow rate compared to the air mass flow rate, the effects on the energy balance of the stack would be negligible. On the other hand, with a smaller heat exchanger in EC mode, the inlet steam cannot receive an appropriate pre-heating. For example, if the size of HX-F-HT is reduced to lower the fuel inlet temperature from 745 °C to 700 °C, the steam flow would be pre-heated to 629 °C instead of 667 °C. To avoid excessive gradients within the stack (by respecting the assumed 100 °C in-out difference), additional heat would be required by the fuel heater. This would translate into an efficiency drop of 0.8 %, if an electrical pre-heater is considered. On the other hand, an excessive mismatch in the fuel and air side inlet temperature could be problematic for internal temperature gradients and material integrity. In this matter, further investigations with more detailed rSOC models could be required.

5. Partial load results

The regulating strategies presented above are used to compute the performances of the system at different steady-state operating points in both modalities. The results are presented first for the fuel cell mode operation and then for the electrolysis one. In both cases, the analysis starts from the electricity consumption of the main BoP components, and then it looks at how they affect the system efficiency. Finally, the extent of the heat recovery and the heat request from the thermal energy storage throughout the partial load operating window is discussed. The streams properties and the TQ diagrams of the system at 50 % part-load conditions are shown in the Supplementary Materials.

5.1. Fuel cell mode

In fuel cell mode, the system current density is varied from the design value of 0.5 A/cm^2 to a value of 0.1 A/cm^2. This variation in current density translates to a considerable reduction in the generated heat within the rSOC module and the required circulating air mass flow rate. In this case, the nominal air mass flow rate of 6.1 kg/s reduces to 0.8 kg/s at the minimum current density. This strong reduction in the required air flow is handled by modulating each fan equally up to their technical limit of 30 % of the nominal air flow rate, and then shutting down one fan at a time.

Fig. 3 shows the electrical power consumption of the main BoP components, namely the air blowers, the fuel blower, and the auxiliary for heat rejection, at different system power levels. The fuel blower and other auxiliary units have a minor impact on the BoP consumption, corresponding to 4 % of the net system power output at nominal load. Such impact increases when reducing the load, reaching 22 % of the total BoP consumption at minimum load (of which, 18 % pertains to the auxiliary). For air circulation, three fans are used from 100 % to 53 % of the system electrical power, two fans up to 39 %, and one fan to cover the last portion of the operating window. When one fan is shut down, the remaining ones experience a sudden increase in the processed air flow. This translates in an increased prevalence given by the blower, and consequently an increased electrical power consumption. The use of

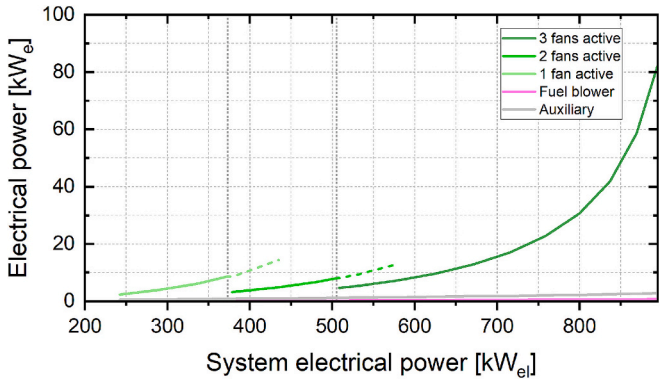

Fig. 3. Electrical consumption of the BoP components, as a function of the net electrical power output, in FC mode. Solid lines show the consumption of the fans when optimally operated, dashed lines show what would be the consumption of one fan or two fans when operated at loads where the operation with two or three fans, respectively, is theoretically optimal.

variable speed fans enables a substantial reduction in electricity consumption at lower loads. In particular, at the minimum load, the reduction accounts to 94 % with respect to the nominal consumption. The deterioration of the electric motor and VFD efficiencies has therefore a negligible effect. What is shown in Fig. 3 assumes that it is always possible to determine at any instant what is the optimal utilization of the fans. This implies that it is always possible to split the total flow rate to the highest number of fans, while respecting their minimum technical limit. In reality, control systems are more complex and do not instantly react to a system perturbation. Therefore, dashed lines in the figure show what would be the consumption of one fan or two fans when operated at loads where the operation with two or three fans, respectively, is instead theoretically optimal. In these cases, the consumption of the fans is higher, as they are required to process a higher air mass flow rate compared to the optimal case. Nevertheless, differences remain limited, if compared to the consumption at the nominal load.

Fig. 4 displays the system efficiency variation when decreasing the load of the system. When reducing the load, the system efficiency follows the increase in stack efficiency that is common in electrochemical systems, and it reaches a value of 76.4 % when operated at the minimum load. In particular, the increase in system efficiency is prominent close to the nominal load, due to the strong reduction of the air fans' electrical consumption, reducing from almost 5 % at the nominal load, to less than 1 % below 50 % of the load. Other significant losses are related to the inverter operation, which account for 1–2 % of the total power consumption. Losses related to the fuel blower and the auxiliary are grouped together as their influence is negligible.

Finally, the deep reduction in heat generation within the stack influences also the heat that can be recovered from the air side. Fig. 5 shows the thermal power that is released to the molten salts in fuel cell mode at different power levels. The thermal power recovery follows the same trend of the heat generation within the stack and the circulating air mass flow rate. At the minimum load, the thermal power output accounts to 49 kW, against the 502 kW of the nominal load. The temperature of the air exhaust that is released in the atmosphere keeps always below 60 °C and decreases up to 30 °C at the lowest load, indicating the heat content in the air stream is efficiently extracted throughout the operating window.

5.2. Electrolysis mode

In electrolysis mode, the current density is varied from the nominal value of 0.81 A/cm^2 to a minimum of 0.12 A/cm^2. To allow a wide operating window of the system in this modality, three regulating strategies have been employed to regulate the heat extraction/provision to the rSOC module during exothermic operation, close to the thermoneutral point, and in the endothermic region. Especially for the latter, the use of additional heaters is essential to cope with the high request of high-temperature heat, which can be computed by means of Eq. (21) [52]. Fig. 6 shows the required thermal power by the reaction as a function of the rSOC stack load. When the operation is exothermic, the endothermic power is negative, meaning that excess thermal power is generated and must be removed by the incoming air flow. This excess reduces considerably when approaching the thermoneutral point, after which the thermal power switches to positive values, and high-temperature heat must be provided to the rSOC module, through heaters. When the stack power is further reduced, the required thermal power reaches a maximum value and then approaches zero again as the extent of the reaction goes to zero as well.

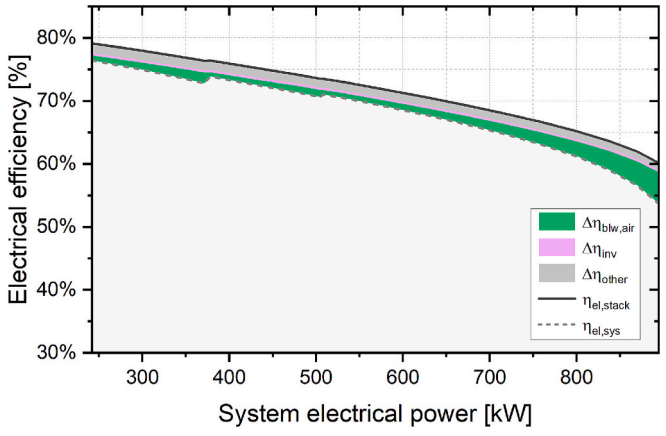

Fig. 4. System electrical efficiency and system efficiency losses, as a function of the net system electrical power output, in FC mode.

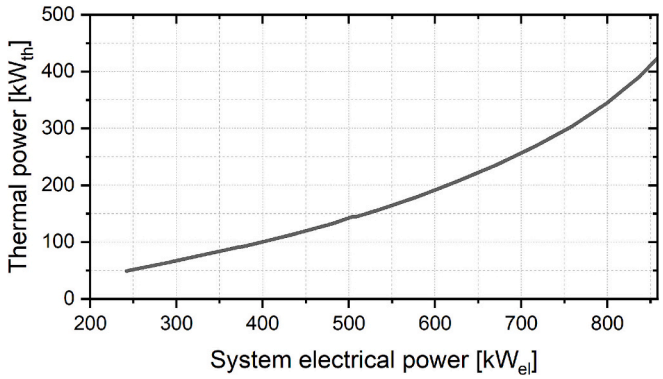

Fig. 5. Thermal power recovery, as a function of the net system electrical power output, in FC mode.

$$\dot{Q}_{endo} = j \cdot (V_{TN} - V) \cdot A \tag{21}$$

In this context, four different configurations for the high-temperature heaters are compared, as anticipated in Section 2. First, the BoP electrical consumption for the Pre-EH and Pre-HC configurations is presented, highlighting the contributions of the main components, such as the air fans and the heaters, identifying the specifying rages for the three strategies throughout the operating window. Second, the request of high-temperature heat for all four configurations is compared and plotted with respect to the stack power consumption and the system power consumption. Finally, the net thermal power input and system electrical efficiency is compared for all four configurations.

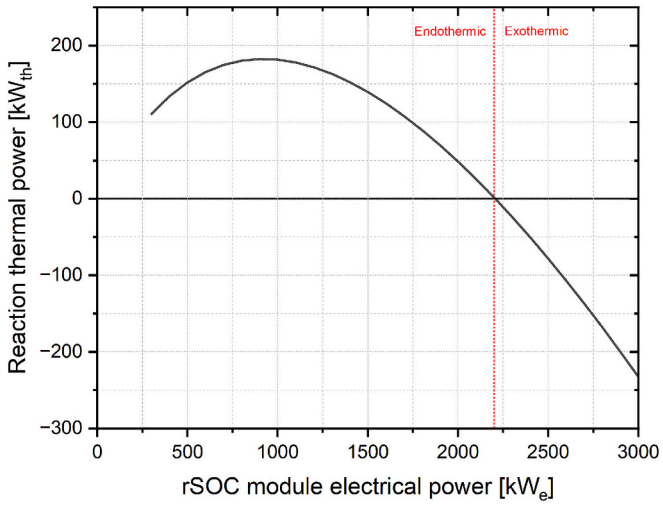

Fig. 6. Thermal power request of the electrolysis reaction in the endothermic region (positive) and thermal power generation in the exothermic region (negative), as a function of the rSOC stack load, in EC mode.

Fig. 7 shows the electrical consumption of the main BoP components throughout the available operating window, for the configuration with the electric pre-heater and the pre-combustor. In both cases, when the reaction is exothermic, Strategy A is employed, where the air mass flow rate is regulated to extract the excess heat of the reaction. The power consumption of the air blower reduces sharply, until its technical limit is reached. In EC mode, being the circulating air flow considerably lower than that required for the FC mode, one fan is sufficient. Moreover, to ensure that the fuel inlet temperature equals that of the air inlet flow to the stack, the fuel electrical heater is used. Differently than in FC mode, the fuel exhaust flow has a lower thermal capacity than the fuel inlet flow (due to the transfer of oxygen ions to the air side), thus making it impossible to pre-heat the inlet flow to the desired temperature. When the technical limit of the fan is reached, the air mass flow rate is fixed to the minimum that can be processed by the fan, and *Strategy B* is employed. During this phase, the air side heater is activated to regulate the temperature of the rSOC stack and avoid its unwanted cooling. *Strategy B* is used across thermoneutral point: during this phase, as the current density is reduced, the temperature of the fuel and air flows increases, reaches and surpasses the outlet temperature of 750 °C. As the current density is reduced further, the maximum temperature of 850 °C at the inlet of the stack is reached, and *Strategy C* must be employed to avoid surpassing this limit. The inlet temperature is fixed to 850 °C, and the additional heat that is required by the electrolysis reaction is provided by increasing the air mass flow rate, leading to an increase in the consumption of the air blower as well. In this phase, the differences between the two configurations can be appreciated. In the Pre-EH configuration, a significant increase in the air electric heater consumption is observed, which derives from the increase in air mass flow rate. Differently, the fuel electric heater, given the decreasing fuel flow rate, requires decreasing electrical power to bring the fuel flow to the inlet temperature of 850 °C. On the other hand, in the Pre-HC configuration, the total consumption of the BoP is substantially lower throughout the operating window, given that the high-temperature heat is provided via combustion of part of the produced hydrogen. In both cases, the air fan consumption follows the trend of the requested thermal power of Fig. 6. The air mass flow rate is always below 2 kg/s, and therefore the need to use additional fans is not required. In the Post-EL and Post-HC configurations the same trend of BoP electricity consumption can be observed, and therefore will not be discussed further.

Fig. 8 shows the high-temperature heat provision from the air and fuel heaters in all four configurations, when compared at equal stack power. In the case of hydrogen-fed combustors, the provided heat is computed via the lower heating value of the H_2 flow that is diverted from the fuel exhaust to the combustor. Heaters that are placed after the stack always provide a larger thermal power with respect to their pre-heaters counterparts. When post-heaters are employed, in fact, the inlet air and fuel flows are brought to the same inlet temperature as in the pre-heater configurations, but at the expense of the exhaust flows cooling. To do so, the post-heaters must bring the exhaust flows to a higher temperature, and therefore they provide excess thermal power with respect to the pre-heaters configurations. On the other hand, electric heaters and combustors provide the same amount of thermal power, since the endothermic power required by the reaction is the same with equal stack power. Nonetheless, as shown with the BoP analysis, electric heaters and combustors have a different effect on the BoP consumption and consequently on how they affect the system electrical power. Similarly, while providing the same thermal power to the stack, the combustors subtract a significant fraction of the generated hydrogen, thus reducing the net output of the system in EC mode. To properly assess the performances of electric pre-heaters and H_2 pre-combustors, one must take into account the trade-off of reducing the net H_2 output

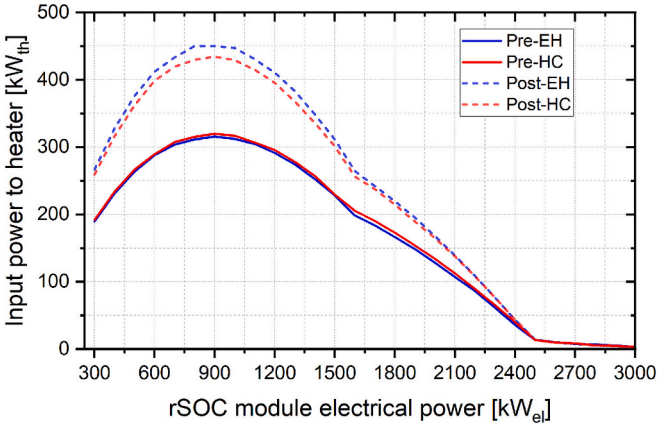

Fig. 8. High-temperature heat provision to the air and fuel sides, as a function of the stack electrical power consumption, in EC mode, for all four configurations.

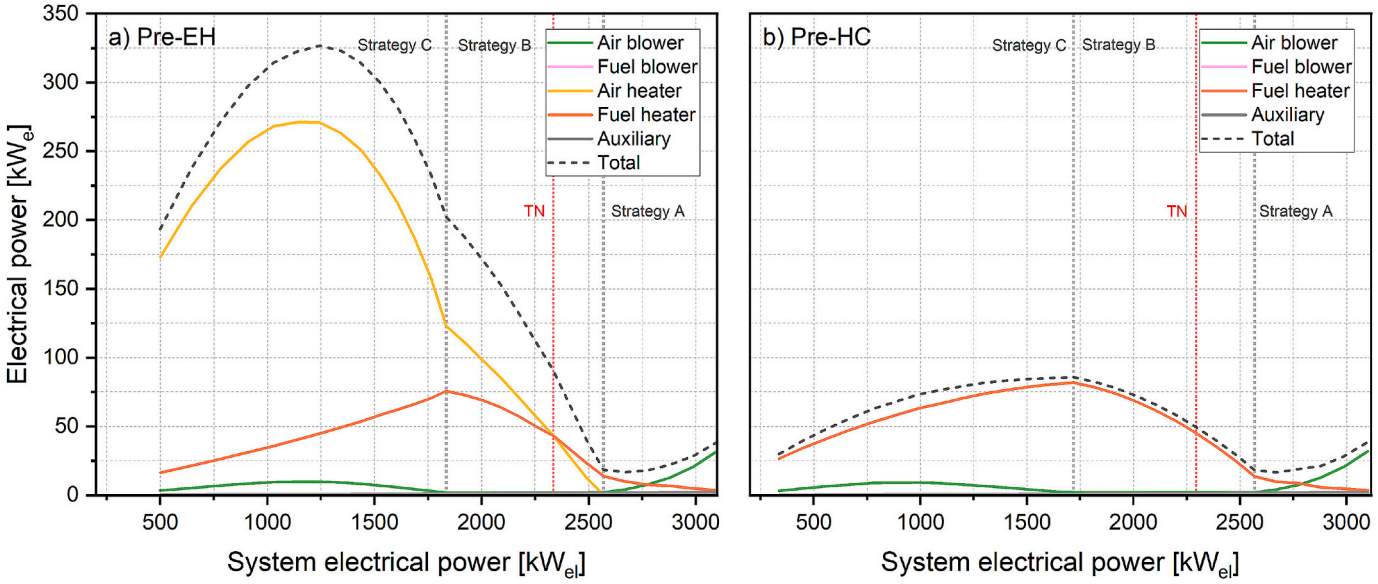

Fig. 7. Electricity consumption of the main BoP components, as functions of the system electrical power consumption, in EC mode, for the Pre-EH and Pre-HC configurations.

and increasing the total electrical input, for the combustors and electrical heaters respectively.

Fig. 9 shows the net hydrogen output and the system electrical efficiency of the system of all four configuration, when compared at a given system net electrical power. As already noted before, due to the excess high-temperature heat provision, the post-heater configurations are characterized by a lower net hydrogen production and system efficiency throughout the operating window. On the contrary, the pre-heaters configurations achieve a comparable net hydrogen output throughout a good portion of the operating range, except for very lower loads. In particular, below 1200 kW of system electrical power, more than 20 % of the produced hydrogen in the stack is burned in the combustor, reaching values higher than 40 % for the lowest bound of the operating map. In this regard, it appears that for low values of hydrogen generation (and total electricity consumption), the drawback of internally consuming a higher fraction of the generated hydrogen surpasses the benefit of saving electricity. This effect is clearly more appreciable when looking at the system efficiency. At the lower operating bound of the Pre-EH configuration (500 kW), the system efficiency of the Pre-HC configuration is almost 8 % lower. Nevertheless, it must be noted that the higher BoP consumption of the Pre-EH configuration reduces its available system power operating window, whose lower boundary is reduced by almost 200 kW.

A detailed breakdown of the system efficiency losses for the main BoP components is shown in Fig. 10 for the two pre-heaters configurations. At the operating window lower bounds, the two cases achieve system efficiencies of 80.2 % and 70.0 %, respectively. By large, the main contribution to the system efficiency losses derives from the heaters placed on the air side, which accounts to 46 % and 49 %, respectively. The fuel electric heater in the Pre-HC configuration is characterized by a higher system efficiency loss throughout the whole operating window, with respect to the Pre-EH configuration. Due to the extraction of a fraction of the exhaust gases from the fuel side, a higher thermal power input is required by the fuel heater in the Pre-HC mode to bring the fuel inlet to the same temperature of the air inlet. In general, the main drivers for the system efficiency losses are those related to thermal power request of the endothermic reaction. Losses related to the air and fuel blower, to the rectifier and to the auxiliary are minimal, and in total they never exceed 4 %.

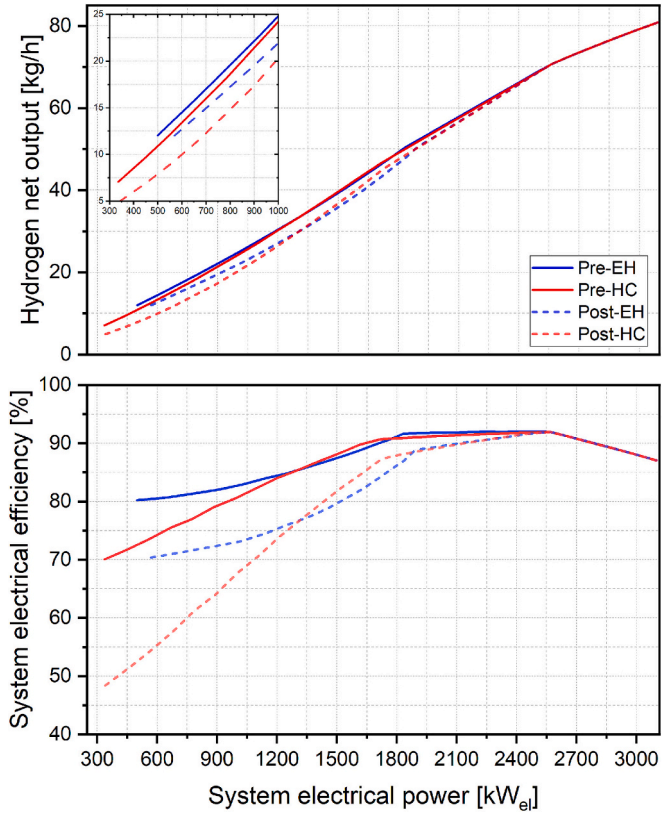

Fig. 9. Net hydrogen output (top) and system electrical efficiency (bottom), as functions of the system electrical power consumption, in EC mode, for all four configurations.

The net thermal power request of the system in EC mode is a result of the total request for water evaporation and the thermal power that can be recovered from the air exhaust. Fig. 11 shows these two contributions as functions of the system power level, for the two pre-heaters configurations. The differences stem from the already discussed discrepancies in the total BoP consumption. In general, the fuel thermal power request for water evaporation follows a decreasing trend, since the constant utilization factor permits to considerably reduce the circulating water mass flow rate in the system. On the contrary, the thermal power that can be recovered along the air side follows different trends depending on the utilized strategy. When *Strategy A* is employed, the thermal power recovery reduces when reducing the system power, as observed for the FC mode. While *Strategy B* is employed, the recovered power is almost fixed as the air mass flow rate is kept constant to the minimum value that can be accepted by the fan. As *Strategy C* is used, when a fully endothermic reaction takes place, the recovered thermal power follows the same trend of the circulating air mass flow rate, which follows in turn the trend of the required endothermic power by the reaction.

In the end, the net thermal power request of all four configurations is compared in Fig. 12. In all cases, when *Strategy A* is employed during the exothermic operation, the net request slightly increases as the system power is decreased. This is because the reduction of thermal power recovery on the air side is sharper than the reduction of thermal power required for water evaporation. On the other hand, with the onset of *Strategy B*, the air mass flow rate is fixed, and the net thermal power starts to reduce with the system electrical power. A change in slope is then observed for the last region of the operating window, where the air mass flow rate is again regulated and contributes largely to reduction of the net request of molten salts. In general, the possibility of recovering thermal power from the air side even in electrolysis mode is beneficial for the system, as it reduces significantly the net consumption of molten salts from the storage, especially for system loads close to the nominal one. The excess thermal power of the heaters that is not utilized by the reaction can be in part recovered along the air side. This is true especially for the post-heaters cases, where at low system loads it even surpasses the one required for water evaporation.

The heat recovery is less efficient in electrolysis mode than in fuel cell mode, because of the higher thermal capacity of the air exhaust flow (in this case, oxygen ions are transferred from the fuel side to air side). Nevertheless, the air exhaust temperature from the low-temperature air pre-heaters never exceeds 100 °C when *Strategy B* is employed (when the air mass flow rate is not regulated), and it reaches values as low as 50 °C when *Strategy C* is employed (when the air mass flow rate is regulated).

6. Discussion

6.1. Comparison with other numerical works

The results of the nominal operation of the system with the assumed operating conditions shows a FC mode system efficiency of 53.7 % and an EC mode system efficiency of 87.0 %. This translates into a roundtrip system efficiency of 46.1 %. The available literature studies (see Section 1.1) report a wide range of roundtrip efficiencies: systems relying on syngas mixtures span from 52.9 to 79.9 %, with an outlier at 37.5 %, whereas systems relying on steam/hydrogen exhibit values from 47.4 to 60 %. The differences between the two sets of systems (syngas mixtures or hydrogen/steam) are mainly attributable to the choice of the fuel: especially when other reactions are involved within the stack (e.g., methanation), the net heat required by the reaction can be strongly

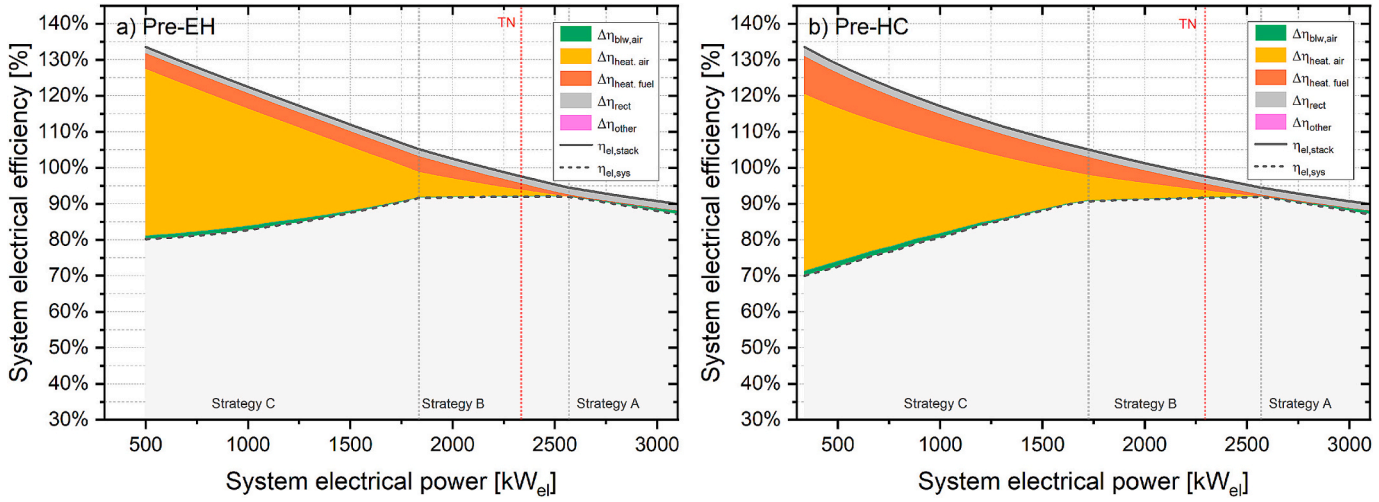

Fig. 10. System electrical efficiency (left) and system efficiency losses (right), as functions of the electrical power consumption, in the EC mode, for the Pre-EH and Pre-HC configurations.

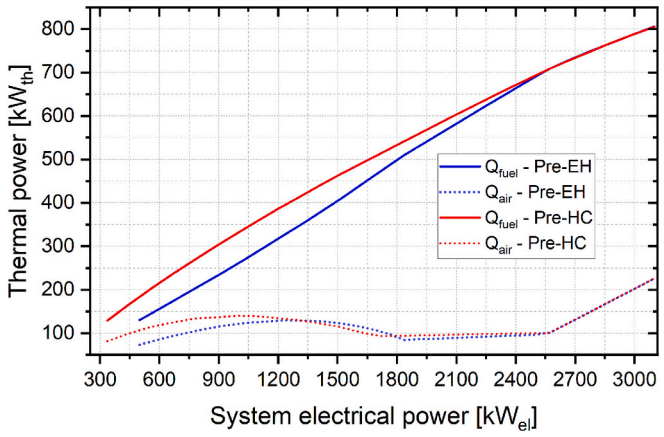

Fig. 11. Thermal power request for water evaporation (solid lines) and recovered thermal power from the air exhaust (dotted lines), as functions of the system electrical power consumption, in EC mode, for the Pre-EH and Pre-HC configurations.

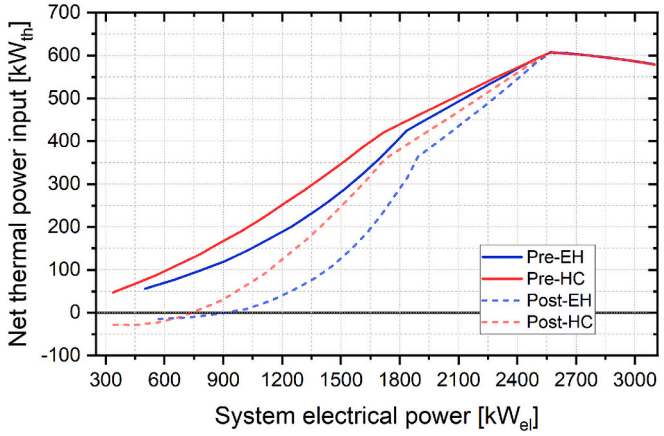

Fig. 12. Net thermal power input, as a function of the system electrical power consumption, in EC mode, for all four configurations.

reduced, if not eliminated. This work shows that the endothermic operation of the system can be detrimental to the system efficiency, due to the large amount of heat to be provided at high temperature.

Differences emerging within works that studied hydrogen-steam rSOC systems are mainly attributable to the choice of the operating conditions, to the availabilities of external heat sources, but also to differences in the experimental results used to represent the rSOC performances. Systems operating with nominal voltages closer to the OCV exhibit higher stack roundtrip efficiencies. Voltages closer to the OCV may depend on the choice of the nominal current densities, or to more efficient cells. Solid oxide cells are still in their development phase; hence, non-negligible differences between performances of different cells may exist. In this work, nominal operating voltages of 0.76 V in FC mode and 1.39 V in EC mode are considered. These depend on the set of experimental curves used to describe the operation of the system (i.e., the assumptions of the OCV and the ASR), and on the assumed nominal current densities. At both stack and system levels, this translates into a lower electrical roundtrip efficiency, lying in the lower range of the cited works. At the same time, a less efficient operation translates into a larger heat generation, which is indeed another useful effect of the system. If this is included in the efficiency calculation (computing the first-principle efficiency as defined in Section 3.5), the system in FC mode achieves an efficiency of 83.1 %. Heat recovery can be crucial in rSOC systems, as it can reduce the external heat request in EC mode, thus increasing its system efficiency. The trade-off between electrical efficiency and heat recovery is complex, and cannot be completely addressed with the analyses carried out in this work. Further studies, considering the long-term operation of rSOC systems in real-world scenarios are required to investigate this topic.

The difference between the stack and system efficiency is useful to isolate the effects of the BoP. In this work, a difference of 6.5 percentage points is observed, which is almost exclusively attributable to the air fan consumption. On the other hand, Frank et al. [15] and Wang et al. [17] reported differences of 27 and 14 percentage points, respectively, at nominal load. These are driven by the large consumption of the electric heaters in EC mode to enable the endothermic electrolysis. In the second case, despite the lower voltage (1.11 V vs. 1.19 V, corresponding to larger high-temperature heat requirements), the system is characterized by a higher roundtrip efficiency: employing hydrogen expanders in FC mode allows to generate positive power output, thus reducing the BoP consumption. A similar approach is used by Perna et al. [16], where they combined upstream hydrogen expansion in FC mode to thermoneutral electrolysis operation in EC. This enables a reduction in both the net electric input and the required high-temperature heat, yielding a

difference in the roundtrip efficiency at stack and system level below 3 percentage points. The advantage of operating close to theoretical thermoneutral conditions is observed also in the partial-load trends of this work, as those conditions cover the area of highest system efficiencies.

6.2. Operational maps of the system

While it is important to optimize the operating parameters at nominal load to maximize the roundtrip efficiency, it is important to explore the system efficiency of both modes throughout their partial load range. In this regard, different strategies are investigated to provide high-temperature heat during the endothermic electrolysis (which is shown to be affected by the largest system efficiency losses).

The comparison of the different heater configurations shows how the most efficient choice is to place the heaters before the stack. Directly increasing the temperature of the inlet flows permits to limit the excess thermal power that is generated when enabling the endothermic reaction. Instead, among the pre-heating configurations, the hydrogen pre-combustor represents an interesting option from the nominal load to the mid-power levels of the EC mode. Differently, the electric pre-heater has a milder impact on the system efficiency at particularly low system loads. The use of electric heaters translates into a considerable impact on the total BoP consumption, thus reducing the available operating window with respect to the pre-combustor option. Nevertheless, the thermal power that is required at the rSOC stack level shows a decreasing trend for particularly low current densities. As a consequence, this translates into a decreasing BoP electricity consumption for the Pre-EH case, which could possibly reduce the limitations in the available operating window for current densities lower than what shown in this work.

The possibility to recover heat from the air exhaust in electrolysis mode can reduce consistently the net thermal power requirements for water evaporation. At nominal load, despite the differences in the system power between the two modalities, the extent of heat recovery in fuel cell mode at nominal load is comparable to the extent of the heat request in the nominal operation for the EC mode. However, the amount of recoverable thermal power in FC mode experiences a sharp decline, consistently with the trend of the generated heat inside the stack. Simultaneously, the nominal hydrogen generation in EC mode is almost double than that required in FC mode to generate power. In this regard, it appears of interest to show how the recoverable and required thermal power in FC and EC modes evolve with respect to their system power load. The same can be done for the hydrogen net output and input in the two modalities. Fig. 13 shows the operating maps (hydrogen input/output and net thermal exchange with the molten salt storage) in FC mode and EC mode (Pre-EH configuration). With the rSOC stack power ratio of 3:1 assumed in this work, the rSOC system run in EC mode can produce a substantial larger amount of hydrogen throughout the whole operating window, with respect to that required for the FC mode operation. To do so, the rSOC system in EC mode requires a significant amount of thermal power. The limited difference in thermal power requirement/recovery observed between the two modalities at nominal load enlarges significantly at medium system loads, while it becomes again comparable at low loads.

In the end, for the proposed system to be thermally self-sufficient on the water evaporation side, the rSOC should run for longer times in FC mode at consistently high system loads. Alternatively, when operated in EC mode, the rSOC should be operated at limited current densities to reduce the thermal power requested from the molten salt storage. In this regard, the adoption of clean sources to generate low-temperature heat (e.g., concentrating solar thermal technologies), could be beneficial in reducing the thermal load for water evaporation. Nevertheless, the optimal scheduling of an rSOC system operation is influenced by the availability of renewable energy sources, the profiles of end-use demands (hydrogen and electricity, for example), and the capacities of the hydrogen and molten salt thermal storage.

6.3. Alternative heat transfer fluids

The selected heat transfer fluid to enable the thermal integration (i.e., solar salt) is derived from common CSP applications and chosen for its proven track of records. Nevertheless, given the limited evaporating temperature of water, different fluids can be selected, like diathermal oil, which operate at lower temperatures with reduced risk of solidification. However, it must be noted that the selection of the heat transfer fluid, and eventually its operating temperature, does not alter the observed trends in the performances of the system and its part-load operation, while it yields different sizing of the heat exchangers, hence impacting the economics.

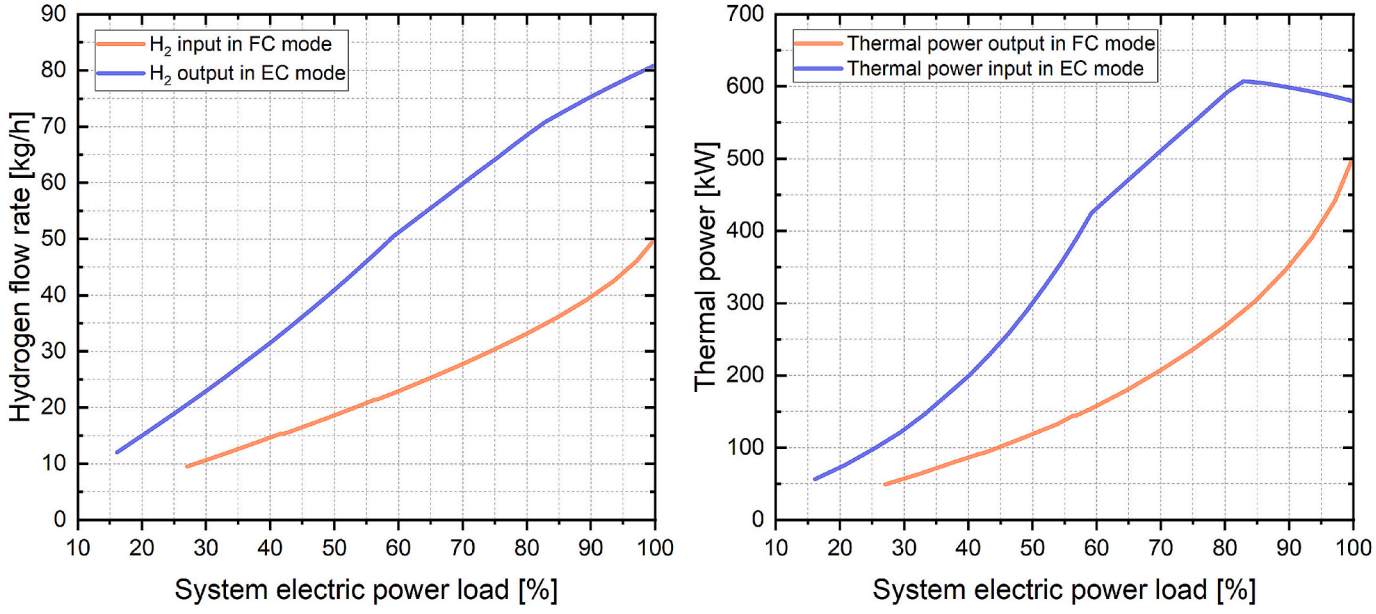

Fig. 13. Operating maps of the rSOC system in FC mode and EC mode with the Pre-EH configuration.

6.4. Limitations of the work

A limitation of this work lies in the modelling assumptions used for the rSOC stack. Employing a 0D model does not describe the effects of uneven internal heating (exothermic operation) or cooling (endothermic operation) that lead to variable local cell temperatures at different operating loads. Moreover, the effect of a constant reactant utilization factor and variable feed flow rates at different power levels at a cell level is not considered. Both these phenomena could affect the actual operating voltage at lower system loads, and therefore the overall system efficiency and heat generation. However, modelling these phenomena with higher spatial resolution (e.g., 1D) opens the way to a different level of detail: this would fall out of the scope of this study that has aimed at investigating BoP configurations to compare thermal integration options.

Another element impacting on the analysis is the use of polarization curves derived from standard experimental procedure, i.e., testing in furnaces with constant temperature and constant feed flows in each mode of operation. This study mitigated this by selecting tests on short stacks rather than single cells, given that data on adiabatic rSOC stacks are not available. Moreover, input data refer to different inlet compositions in the two modalities, close to those simulated. At any rate, the calculations for the FC mode can be considered conservative regarding the electrical efficiency. Its simulated inlet composition assumes slightly lower steam presence (2 $\%_{mol}$) than the conditions of the experimental tests (10 $\%_{mol}$ H_2O – 90 $\%_{mol}$ H_2) [39], which would lead to an upward translation of the polarization curve, favored by a higher OCV. Finally, further updates of the analysis could be done by considering more advanced cell specifications with respect to those assumed in this work, which may allow to achieve an improved performance in terms of cell voltage (e.g., fuel cell operation at 0.82-0.85 V, as observed in some recent developments) and thus improved efficiency.

7. Conclusions

In this work, a reversible solid oxide cell system based on steam electrolysis and hydrogen feeding has been modelled and simulated using the Aspen Plus® software. The system is characterized by a unified balance of plant that supports the reversible operation of the system, and it is coupled with a thermal energy storage system based on molten salt. The adoption of intermediate thermal storage enables the recovery of excess thermal power in FC mode, which helps in reducing the external heat supply for water evaporation and steam superheating in EC mode. Different strategies to allow a wide window of partial-load operation of the system in both modalities have been proposed and studied. Particularly for the EC endothermic region, electric heaters or hydrogen combustors placed at the stack inlet or outlet have been compared.

The main conclusions of the work can be summarized in the following points:

(i) The air flow rate required to extract the excess thermal power in FC mode is considerably higher than that required in EC mode. Moreover, the air flow rate required in FC mode reduces sharply when decreasing the load. The use of multiple variable-speed fans placed in parallel allows to efficiently handle such large variations.

(ii) The system electrical efficiency in FC mode is 53.7 % at nominal load, with the predominant system efficiency loss stemming from the air blower (4.9 %). At the minimum load of 24 %, the system efficiency increases to 76.4 % as a combination of increased stack efficiency and decreased air blower consumption.

(iii) In EC mode, without considering the hydrogen compression, the system electrical efficiency at nominal load is 87.0 %. The highest system efficiency (91.7 %) is achieved close to the thermoneutral point: operating points within the exothermic region suffer from decreased stack efficiency, while points in the endothermic region from excessive efficiency losses due to high-temperature heat provision. Therefore, the benefits of running the electrolysis reaction at lower voltages cannot be fully exploited, unless external waste heat at high temperature is available. Nevertheless, with the best configuration, the system efficiency spans within a limited range (80–90 %) over the entire operating window.

(iv) Other than enabling a deep endothermic operation, high-temperature heat provision can serve as an effective regulating mechanism in regions that are not theoretically endothermic. As shown with *Strategy B*, where air modulation is not feasible due to technical limits of the machines, external heat provision is required to avoid an excessive cooling of the stack.

(v) Among the compared EC mode configurations, those that provide heat directly before the stack are characterized by the highest efficiency throughout the operating window. In fact, post-heaters provide excess heat with respect to pre-heaters to obtain the same inlet conditions. Among the pre-heaters configuration, the electric option achieves the best system electrical efficiency (80.2 % at the minimum load of 16 %). Nevertheless, the option with a pre-combustor achieves a comparable system efficiency down to 30 % of the system load. This is achieved thanks to a reduced BoP electrical consumption, but a lower net hydrogen output. In this regard, the system efficiency losses formulation defined within this work can prove useful in comparing heat provision configurations that do not rely solely on additional electricity consumption.

(vi) The thermal exchange of the rSOC system with the molten salt thermal storage is comparable for the two modalities at their respective nominal loads. Nevertheless, the heat recovery in FC mode at lower loads reduces faster than the net heat request in EC mode. To operate the system without external low-temperature heat sources, an unbalanced operation between the two modalities may be required (longer duration in FC mode at higher loads and/or lower duration in EC mode at lower loads).

The results of this work show some of the potential issues in handling the thermal integration between the two operating modalities of rSOC systems when aiming to exploit their whole operating window. The system efficiency in EC mode appears to be largely affected by the use of additional heaters. In this regard, future work may explore system modifications that can help in reducing the requirements of external heat sources, such as concentrating solar thermal for water evaporation or the use of high-temperature storage to enable endothermic electrolysis. The operating maps will be used to represent the rSOC operating patterns in the investigation of multi-energy systems over the long run, when integrated with intermittent renewable energy sources and variable end-use demands.

There is wide evidence on the performances of solid oxide cells in laboratory environment, where experiments are conducted at controlled temperature. However, experimental investigation of full rSOC systems that are thermally self-sustaining has not been extensively addressed. While this work may be useful in predicting the performance of such systems over wide operating ranges, it is of primary importance that the results are experimentally verified. Future work and projects should therefore move in this direction.

CRediT authorship contribution statement

Marco Ficili: Writing – original draft, Visualization, Software, Methodology, Investigation, Formal analysis. **Paolo Colbertaldo:** Writing – review & editing, Software, Methodology, Investigation, Conceptualization. **Stefano Campanari:** Supervision, Funding acquisition, Conceptualization. **Giulio Guandalini:** Investigation, Conceptualization, Writing – review & editing.

Declaration of competing interest

The authors declare that they have no known competing financial interests or personal relationships that could have appeared to influence the work reported in this paper.

Acknowledgments

This work has been developed within the project 'High Efficiency Reversible technologies in fully renewable Multi-Energy System' (HERMES). The project has received funding from the Italian Ministry of Education, University, and Research (MIUR), as Research Project of Relevant National Interest PRIN 2017F4S2L3.

Appendix A. Appendix

In this appendix, the definitions of the system efficiency losses with respect to the stack efficiency defined in Section 3.5.3 are demonstrated in detail for the FC and EC modes.

A.1. Fuel cell mode

$$\eta_{stack,FC} = \frac{P_{stack}}{\dot{m}_{H_2,cons} \cdot LHV_{H_2}}$$

$$\eta_{el,sys,FC} = \frac{P_{el,net}}{\dot{m}_{H_2,in} \cdot LHV_{H_2}}$$

$$P_{el,net} = P_{stack} \cdot \eta_{inv} - \sum P_{BOP,i}$$

In FC mode, system losses are related mainly to the electricity consumption of the BoP components $P_{loss,i}$ and will be referred to as $\Delta\eta_{i,el,FC}$:

$$\Delta\eta_{i,el,FC} = \frac{P_{loss,i}}{\dot{m}_{H_2,in} \cdot LHV_{H_2}}$$

The only loss attributable to hydrogen is the purge loss:

$$\Delta\eta_{H_2,purge} = \eta_{stack,FC} \cdot \frac{\dot{m}_{H_2,purge}}{\dot{m}_{H_2,in}}$$

The system efficiency losses are defined with respect to the stack efficiency, such that:

$$\eta_{stack} = \eta_{el,sys,FC} + \sum \Delta\eta_{i,el,FC} + \sum \Delta\eta_{i,H_2,FC}$$

In the system under study:

$$\Delta\eta_{inv} = \frac{P_{inv}}{\dot{m}_{H_2,in} \cdot LHV_{H_2}}$$

$$(P_{inv} = P_{stack} - P_{stack} \cdot \eta_{inv})$$

$$\Delta\eta_{blw,air} = \frac{P_{blw,air}}{\dot{m}_{H_2,in} \cdot LHV_{H_2}}$$

$$\Delta\eta_{blw,fuel} = \frac{P_{blw,fuel}}{\dot{m}_{H_2,in} \cdot LHV_{H_2}}$$

$$\Delta\eta_{el,heat} = \frac{P_{el,heat}}{\dot{m}_{H_2,in} \cdot LHV_{H_2}}$$

Analytical proof:

$$\Delta\eta_{i,H_2} + \Delta\eta_{i,el} = \eta_{stack} - \eta_{el,sys,FC}$$

$$= \frac{P_{stack}}{\dot{m}_{H_2,cons} \cdot LHV_{H_2}} - \frac{P_{el,net}}{\dot{m}_{H_2,in} \cdot LHV_{H_2}}$$

$$= \frac{P_{stack}}{\dot{m}_{H_2,cons} \cdot LHV_{H_2}} - \left(\frac{P_{stack}}{\dot{m}_{H_2,in} \cdot LHV_{H_2}} - \frac{P_{blw,air}}{\dot{m}_{H_2,in} \cdot LHV_{H_2}} - \frac{P_{blw,fuel}}{\dot{m}_{H_2,in} \cdot LHV_{H_2}} - \frac{P_{inv}}{\dot{m}_{H_2,in} \cdot LHV_{H_2}} - \frac{P_{el,heat}}{\dot{m}_{H_2,in} \cdot LHV_{H_2}} \right)$$

$$= \frac{P_{stack}}{\dot{m}_{H_2,cons} \cdot LHV_{H_2}} - \frac{P_{stack}}{\dot{m}_{H_2,in} \cdot LHV_{H_2}} + \Delta\eta_{blw,air} + \Delta\eta_{blw,fuel} + \Delta\eta_{inv} + \Delta\eta_{el,heat}$$

$$= \frac{P_{stack}}{LHV_{H_2}} \left(\frac{1}{\dot{m}_{H_2,cons}} - \frac{1}{\dot{m}_{H_2,in}} \right) + \Delta\eta_{blw,air} + \Delta\eta_{blw,fuel} + \Delta\eta_{inv} + \Delta\eta_{el,heat}$$

$$= \frac{P_{stack}}{LHV_{H_2}} \cdot \frac{\dot{m}_{H_2,in} - \dot{m}_{H_2,cons}}{\dot{m}_{H_2,cons} \cdot \dot{m}_{H_2,in}} + \Delta\eta_{blw,air} + \Delta\eta_{blw,fuel} + \Delta\eta_{inv} + \Delta\eta_{el,heat}$$

$$= \eta_{stack,FC} \cdot \frac{\dot{m}_{H_2,in} - \dot{m}_{H_2,cons}}{\dot{m}_{H_2,in}} + \Delta\eta_{blw,air} + \Delta\eta_{blw,fuel} + \Delta\eta_{inv} + \Delta\eta_{el,heat}$$

$$= \eta_{stack,FC} \cdot \frac{\dot{m}_{H_2,purge}}{\dot{m}_{H_2,in}} + \Delta\eta_{blw,air} + \Delta\eta_{blw,fuel} + \Delta\eta_{inv} + \Delta\eta_{el,heat}$$

$$= \underbrace{\eta_{stack,FC} \cdot \frac{\dot{m}_{H_2,purge}}{\dot{m}_{H_2,in}}}_{\textbf{Additional hydrogen consumption}} + \underbrace{\Delta\eta_{blw,air} + \Delta\eta_{blw,fuel} + \Delta\eta_{inv} + \Delta\eta_{el,heat}}_{\textbf{Missed electricity generation}}$$

$$= \eta_{stack,FC} \cdot \sum \frac{\dot{m}_{loss,i}}{\dot{m}_{H_2,in}} + \sum \frac{P_{loss,i}}{\dot{m}_{H_2,in} \cdot LHV_{H_2}}$$

A.2. Electrolysis mode

$$\eta_{stack,EC} = \frac{\dot{m}_{H_2,prod} \cdot LHV_{H_2}}{P_{stack}}$$

$$\eta_{el,sys,EC} = \frac{\dot{m}_{H_2,out} \cdot LHV_{H_2}}{P_{el,tot}}$$

$$P_{el,tot} = \frac{P_{stack}}{\eta_{rect}} + \sum P_{aux,i}$$

The system losses in EC mode can be related to *additional electrical consumptions* (e.g., BoP electricity consumption, but also the additional electrical consumption due to the rectifier loss) or to *missed hydrogen exports* of the system (e.g., hydrogen consumed in a hydrogen-fed combustor).

- Additional electrical consumptions:

$$\Delta\eta_{i,el} = \eta_{stack} \cdot \frac{P_{add,i}}{P_{el,tot}}$$

- Missed hydrogen exports:

$$\Delta\eta_{i,H_2} = \frac{\dot{m}_{H_2,i} \cdot LHV_{H_2}}{P_{el,tot}}$$

Such that:

$$\eta_{stack,EC} = \eta_{el,sys,EC} + \sum \Delta\eta_{i,el} + \sum \Delta\eta_{i,H_2}$$

In the system under study:

$$\Delta\eta_{rect} = \eta_{stack} \cdot \frac{P_{rect}}{P_{el,tot}}$$

$$\left(P_{rect} = \frac{P_{stack}}{\eta_{rect}} - P_{stack} \right)$$

$$\Delta\eta_{blw,air} = \eta_{stack} \cdot \frac{P_{blw,air}}{P_{el,tot}}$$

$$\Delta\eta_{blw,fuel} = \eta_{stack} \cdot \frac{P_{blw,fuel}}{P_{el,tot}}$$

$$\Delta\eta_{el,heat} = \eta_{stack} \cdot \frac{P_{el,heat}}{P_{el,tot}}$$

$$\Delta\eta_{H_2,comb} = \frac{\dot{m}_{H_2,comb} \cdot LHV_{H_2}}{P_{el,tot}}$$

Analytical proof:

$$\Delta\eta_{i,el} + \Delta\eta_{i,H_2} = \eta_{stack} - \eta_{el,sys,EC}$$

$$= \frac{\dot{m}_{H_2,prod} \cdot LHV_{H_2}}{P_{stack}} - \frac{\dot{m}_{H2,out} \cdot LHV_{H_2}}{P_{el,tot}}$$

$$= \frac{\dot{m}_{H_2,prod} \cdot LHV_{H_2}}{P_{stack}} - \left(\frac{\dot{m}_{H_2,prod} \cdot LHV_{H_2}}{P_{el,tot}} - \frac{\dot{m}_{H_2,comb} \cdot LHV_{H_2}}{P_{el,tot}} \right)$$

$$= \frac{\dot{m}_{H_2,prod} \cdot LHV_{H_2}}{P_{stack}} - \frac{\dot{m}_{H_2,prod} \cdot LHV_{H_2}}{P_{el,tot}} + \frac{\dot{m}_{H_2,comb} \cdot LHV_{H_2}}{P_{el,tot}}$$

$$= \dot{m}_{H_2,prod} \cdot LHV_{H_2} \cdot \left(\frac{1}{P_{stack}} - \frac{1}{P_{el,tot}} \right) + \Delta\eta_{H_2,comb}$$

$$= \dot{m}_{H_2,prod} \cdot LHV_{H_2} \cdot \frac{P_{el,tot} - P_{stack}}{P_{stack} \cdot P_{el,tot}} + \Delta\eta_{H_2,comb}$$

$$= \eta_{stack,EC} \cdot \frac{P_{el,tot} - P_{stack}}{P_{el,tot}} + \Delta\eta_{H_2,comb}$$

$$= \eta_{stack,EC} \cdot \frac{P_{blw,air} + P_{blw,fuel} + P_{rect} + P_{el,heat}}{P_{el,tot}} + \Delta\eta_{H_2,comb}$$

$$= \underbrace{\eta_{stack,EC} \cdot \frac{P_{blw,air}}{P_{el,tot}} + \eta_{stack} \cdot \frac{P_{blw,fuel}}{P_{el,tot}} + \eta_{stack} \cdot \frac{P_{rect}}{P_{el,tot}} + \eta_{stack} \cdot \frac{P_{el,heat}}{P_{el,tot}}}_{\text{Additional electrical consumption}} + \underbrace{\Delta\eta_{H_2,comb}}_{\text{Missed hydrogen exports}}$$

$$= \eta_{stack,EC} \cdot \sum \frac{P_{add,i}}{P_{el,tot}} + \sum \frac{\dot{m}_{H_2,i} \cdot LHV_{H_2}}{P_{el,tot}}$$

Appendix B. Supplementary data

Supplementary data to this article can be found online at https://doi.org/10.1016/j.apenergy.2025.125876.

Data availability

Data will be made available on request.

References

[1] Venkataraman V, Pérez-Fortes M, Wang L, Hajimolana YS, Boigues-Muñoz C, Agostini A, et al. Reversible solid oxide systems for energy and chemical applications – review & perspectives. J Energy Storage 2019;24. https://doi.org/10.1016/j.est.2019.100782.

[2] Graves C, Ebbesen SD, Jensen SH, Simonsen SB, Mogensen MB. Eliminating degradation in solid oxide electrochemical cells by reversible operation. Nat Mater 2015;14:239–44. https://doi.org/10.1038/nmat4165.

[3] Hauch A, Pylypko S, Cubizolles G, Mouginn J. Load cycling tests of reversible solid oxide cells – effects of current density, steam content, and utilization, ECS. Meeting Abstracts 2021;MA2021-03:211. https://doi.org/10.1149/ma2021-031211mtgabs.

[4] Baldinelli A, Staffolani A, Nobili F, Barelli L. Detailed experimental analysis of solid oxide cells degradation due to frequent fuel cell/electrolyser switch. J Energy Storage 2023;73:109117. https://doi.org/10.1016/j.est.2023.109117.

[5] Peters Ro, Frank M, Tiedemann W, Hoven I, Deja R, Kruse N, et al. Long-term experience with a 5/15kW-class reversible solid oxide cell system. J Electrochem Soc 2021;168:014508. https://doi.org/10.1149/1945-7111/abdc79.

[6] Peters Ro, Tiedemann W, Hoven I, Deja R, Kruse N, Fang Q, et al. Experimental results of a 10/40 kW-class reversible solid oxide cell demonstration system at Forschungszentrum Jülich. J Electrochem Soc 2023;170:044509. https://doi.org/10.1149/1945-7111/accbf0.

[7] Saarinen V, Pennanen J, Kotisaari M, Thomann O, Himanen O, Di Iorio S, et al. Design, manufacturing, and operation of movable 2 × 10 kW size rSOC system. Fuel Cells 2021;21:477–87. https://doi.org/10.1002/fuce.202100021.

[8] Bierschenk DM, Wilson JR, Barnett SA. High efficiency electrical energy storage using a methane-oxygen solid oxide cell, energy. Environ Sci 2011;4:944–51. https://doi.org/10.1039/c0ee00457j.

[9] Wendel CH, Kazempoor P, Braun RJ. Novel electrical energy storage system based on reversible solid oxide cells: system design and operating conditions. J Power Sources 2015;276:133–44. https://doi.org/10.1016/j.jpowsour.2014.10.205.

[10] Wendel CH, Braun RJ. Design and techno-economic analysis of high efficiency reversible solid oxide cell systems for distributed energy storage. Appl Energy 2016;172:118–31. https://doi.org/10.1016/j.apenergy.2016.03.054.

[11] Mottaghizadeh P, Santhanam S, Heddrich MP, Friedrich KA, Rinaldi F. Process modeling of a reversible solid oxide cell (r-SOC) energy storage system utilizing commercially available SOC reactor. Energy Convers Manag 2017;142:477–93. https://doi.org/10.1016/j.enconman.2017.03.010.

[12] Reznicek E, Braun RJ. Techno-economic and off-design analysis of stand-alone, distributed-scale reversible solid oxide cell energy storage systems. Energy Convers Manag 2018;175:263–77. https://doi.org/10.1016/j.enconman.2018.08.087.

[13] Santhanam S, Heddrich MP, Friedrich KA. Electricity arbitration and sector coupling with an experimentally validated reversible solid oxide cell reactor system connected to the natural gas grid. Energ Technol 2020;8. https://doi.org/10.1002/ente.201900618.

[14] Lonis F, Tola V, Cau G. Renewable methanol production and use through reversible solid oxide cells and recycled CO2 hydrogenation. Fuel 2019;246:500–15. https://doi.org/10.1016/j.fuel.2019.02.108.

[15] Frank M, Deja R, Peters R, Blum L, Stolten D. Bypassing renewable variability with a reversible solid oxide cell plant. Appl Energy 2018;217:101–12. https://doi.org/10.1016/j.apenergy.2018.02.115.

[16] Perna A, Minutillo M, Jannelli E. Designing and analyzing an electric energy storage system based on reversible solid oxide cells. Energy Convers Manag 2018;159:381–95. https://doi.org/10.1016/j.enconman.2017.12.082.

[17] Wang Y, Banerjee A, Wehrle L, Shi Y, Brandon N, Deutschmann O. Performance analysis of a reversible solid oxide cell system based on multi-scale hierarchical solid oxide cell modelling. Energy Convers Manag 2019;196:484–96. https://doi.org/10.1016/j.enconman.2019.05.099.

[18] Giap VT, Kang S, Ahn KY. High-efficient reversible solid oxide fuel cell coupled with waste steam for distributed electrical energy storage system. Renew. Energy 2019;144:129–38. https://doi.org/10.1016/j.renene.2018.10.112.

[19] Giap VT, Lee YD, Kim YS, Ahn KY. A novel electrical energy storage system based on a reversible solid oxide fuel cell coupled with metal hydrides and waste steam. Appl Energy 2020;262:114522. https://doi.org/10.1016/j.apenergy.2020.114522.

[20] Amladi A, Venkataraman V, Woudstra T, Aravind PV. Hot air recirculation enlarges efficient operating window of reversible solid oxide cell systems: a thermodynamic study of energy storage using ammonia. Appl Energy 2024;355:122276. https://doi.org/10.1016/j.apenergy.2023.122276.

[21] Ghezel-Ayagh H. High efficiency reversible solid oxide system (DE-EE0008847). Performance Improvements for Reversible Solid Oxide Fuel Cell Systems 2024; FE0031974.

[22] Sanz-Bermejo J, Muñoz-Antón J, Gonzalez-Aguilar J, Romero M. Part load operation of a solid oxide electrolysis system for integration with renewable energy sources. Int J Hydrog Energy 2015;40:8291–303. https://doi.org/10.1016/J.IJHYDENE.2015.04.059.

[23] Petipas F, Brisse A, Bouallou C. Thermal management of solid oxide electrolysis cell systems through air flow regulation. Chem Eng Trans 2017;61:1069–74. https://doi.org/10.3303/CET1761176.
[24] Ficili M, Colbertaldo P, Guandalini G, Campanari S. Design and partial-load operation of a reversible solid oxide cell system with molten salts thermal storage. J Phys Conf Ser 2022;2385. https://doi.org/10.1088/1742-6596/2385/1/012022.
[25] Bauer T, Pfleger N, Breidenbach N, Eck M, Laing D, Kaesche S. Material aspects of solar salt for sensible heat storage. Appl Energy 2013;111:1114–9. https://doi.org/10.1016/J.APENERGY.2013.04.072.
[26] Wang Y, Li W, Ma L, Li W, Liu X. Degradation of solid oxide electrolysis cells: phenomena, mechanisms, and emerging mitigation strategies—a review. J Mater Sci Technol 2020;55:35–55. https://doi.org/10.1016/j.jmst.2019.07.026.
[27] Mueller F, Jabbari F, Gaynor R, Brouwer J. Novel solid oxide fuel cell system controller for rapid load following. J Power Sources 2007;172:308–23. https://doi.org/10.1016/j.jpowsour.2007.05.092.
[28] Mueller F, Tarroja B, Maclay J, Jabbari F, Brouwer J, Samuelsen S. Design, simulation and control of a 100 MW-class solid oxide fuel cell gas turbine hybrid system. J Fuel Cell Sci Technol 2010;7:0310071–03100711. https://doi.org/10.1115/1.3207868.
[29] Zhou J, Wang Z, Han M. Comparison of three different control strategies for load-change and attenuation of solid oxide fuel cell system. Int J Hydrog Energy 2023;48:30877–86. https://doi.org/10.1016/j.ijhydene.2023.04.171.
[30] Barelli L, Bidini G, Ottaviano A. Solid oxide fuel cell modelling: electrochemical performance and thermal management during load-following operation. Energy 2016;115:107–19. https://doi.org/10.1016/j.energy.2016.08.107.
[31] Aguiar P, Adjiman CS, Brandon NP. Anode-supported intermediate-temperature direct internal reforming solid oxide fuel cell: II. Model-based dynamic performance and control, J Power Sources 2005;147:136–47. https://doi.org/10.1016/j.jpowsour.2005.01.017.
[32] Aguiar P, Adjiman CS, Brandon NP. Anode-supported intermediate temperature direct internal reforming solid oxide fuel cell. I: model-based steady-state performance. J Power Sources 2004;138:120–36. https://doi.org/10.1016/J.JPOWSOUR.2004.06.040.
[33] Petipas F, Brisse A, Bouallou C. Model-based behaviour of a high temperature electrolyser system operated at various loads. J Power Sources 2013;239:584–95. https://doi.org/10.1016/J.JPOWSOUR.2013.03.027.
[34] Srikanth S, Heddrich MP, Gupta S, Friedrich KA. Transient reversible solid oxide cell reactor operation – experimentally validated modeling and analysis. Appl Energy 2018;232:473–88. https://doi.org/10.1016/j.apenergy.2018.09.186.
[35] Motylinski K, Kupecki J, Numan B, Hajimolana YS, Venkataraman V. Dynamic modelling of reversible solid oxide cells for grid stabilization applications. Energy Convers Manag 2021;228:113674. https://doi.org/10.1016/j.enconman.2020.113674.
[36] Liu G, Zhao W, Li Z, Xia Z, Jiang C, Kupecki J, et al. Modeling and control-oriented thermal safety analysis for mode switching process of reversible solid oxide cell system. Energy Convers Manag 2022;255. https://doi.org/10.1016/j.enconman.2022.115318.
[37] Wehrle L, Wang Y, Banerjee A, Brandon N, Deutschmann O. Dynamic modeling of reversible solid oxide cells. Chem Ing Tech 2019;91:833–42. https://doi.org/10.1002/cite.201800188.
[38] Berkel F, Ferchaud CJ, Partenie O, Linders M, van Delft Y. Solid oxide cell technology development at TNO. ECS Trans 2021;103:591–602. https://doi.org/10.1149/10301.0591ecst.
[39] Barelli L, Bidini G, Cinti G, Ottaviano A. Study of SOFC-SOE transition on a RSOFC stack. Int J Hydrog Energy 2017;42:26037–47. https://doi.org/10.1016/j.ijhydene.2017.08.159.
[40] Li N, Wang M, Shen Q, Teng Y, Wang D, Chen C, et al. Reduced concentration polarization and enhanced steam throughput conversion with a solid oxide electrolysis cell supported on an electrode with optimized pore structure. Int J Hydrog Energy 2022;47:21673–80. https://doi.org/10.1016/J.IJHYDENE.2022.05.013.
[41] SolydEra, (n.d.), https://www.solydera.com/it/ (accessed October 3, 2024).
[42] Clean Hydrogen JU - SRIA Key Performance Indicators (KPIs), (n.d.), https://www.clean-hydrogen.europa.eu/knowledge-management/strategy-map-and-key-performance-indicators/clean-hydrogen-ju-sria-key-performance-indicators-kpis_en (accessed November 18, 2024).
[43] Zou Y, Ding J, Wang W, Lee D, Lu J. Heat transfer performance of U-tube molten salt steam generator. Int J Heat Mass Transf 2020;160:120200. https://doi.org/10.1016/j.ijheatmasstransfer.2020.120200.
[44] Liu Z, Wang Y, Xie M, He X, Zhang W, Xie S, et al. Off-design performance analysis for an integrated system of solid oxide fuel cell and supercritical carbon dioxide Brayton cycle with CO2 capture. Energy Convers Manag 2023;292:117406. https://doi.org/10.1016/j.enconman.2023.117406.
[45] Chen R, Romero M, González-Aguilar J, Rovense F, Rao Z, Liao S. Design and off-design performance comparison of supercritical carbon dioxide Brayton cycles for particle-based high temperature concentrating solar power plants. Energy Convers Manag 2021;232. https://doi.org/10.1016/j.enconman.2021.113870.
[46] Zhang F, Feng M, Dai H, Wu Z, Liao G. Off-design and control performance analysis of a novel supercritical carbon dioxide power cycle for waste heat recovery. Appl Therm Eng 2023;235:121393. https://doi.org/10.1016/j.applthermaleng.2023.121393.
[47] Hamilton WT, Newman AM, Wagner MJ, Braun RJ. Off-design performance of molten salt-driven Rankine cycles and its impact on the optimal dispatch of concentrating solar power systems. Energy Convers Manag 2020;220:113025. https://doi.org/10.1016/j.enconman.2020.113025.
[48] Incropera FP, DeWitt DP, Bergman TL, Lavine AS. Fundamentals of heat and mass transfer. Sixth Edition. 2011.
[49] SODECA. https://www.sodeca.com/it/productos/ventilatori-centrifughi-per-applicazioni-industriali-large-series-s47?fil=50; 2023 (accessed October 20, 2023).
[50] AMCA. Estimating part-load performance of fan Motors and drives using AMCA 207. 2025.
[51] Campanari S, Mastropasqua L, Gazzani M, Chiesa P, Romano MC. Predicting the ultimate potential of natural gas SOFC power cycles with CO2 capture – part a: methodology and reference cases. J Power Sources 2016;324:598–614. https://doi.org/10.1016/j.jpowsour.2016.05.104.
[52] Mastropasqua L, Pecenati I, Giostri A, Campanari S. Solar hydrogen production: techno-economic analysis of a parabolic dish-supported high-temperature electrolysis system. Appl Energy 2020;261:114392. https://doi.org/10.1016/j.apenergy.2019.114392.